Y. Geng, C. Li, Y. Guo, J.D. Biggs
Fixed-Time Near-Optimal Control for Repointing Maneuvers of a Spacecraft with Nonlinear Terminal Constraints
ISA Transactions, In press - Published online 30/07/2019
doi:10.1016/j.isatra.2019.07.026

Highlights

1.The notion of repointing maneuver of a spacecraft operating in staring mode is provided.

2.The end conditions of repointing maneuver of a spacecraft both for static target observation and moving target detections are formulated as nonlinear underdetermined equations.

3.The finite-time horizon optimal control strategy is proposed to drive the spacecraft to rotate to the desired orientation at a prescribed time.

4. The waypoint-based SDRE approach improves the control performance and enhances the computational efficiency.

5.The effectiveness and superiorities of the proposed method is verified by numerical simulations.

Fixed-Time Near-Optimal Control for Repointing Maneuvers of a Spacecraft with Nonlinear Terminal Constraints

Yuanzhuo Geng[a,1], Chuanjiang Li[a,2], Yanning Guo[a,3,*], James D. Biggs[b,4]

[a]*Department of Control Science and Engineering, Harbin Institute of Technology, Harbin, 150001, China*
[b]*Department of Aerospace Science and Technology, Politecnico di Milano, 20156 Milan, Italy*

Abstract

Repointing maneuvers of a spacecraft in staring mode are investigated where the optical axis is required to align with the target orientation. Different from traditional three-axis reorientation maneuvers, the rotation about the optical axis is free of constraints for repointing maneuvers. Both static target observation and moving target detection constraints are considered. The problem is then formulated as a finite-time horizon optimal control problem with nonlinear terminal constraints. A simple and efficient state-dependent Riccati equation(SDRE) based dynamic programming approach is applied to tackle this nonlinear optimal control problem. The convergence of the attitude from initial conditions to the desired terminal constraint is rigorously proved for the first time. Considering the inability of the SDRE method to deal with the problem of large angle maneuvers, an im-

*Corresponding author
Email address: gengyz@hit.edu.cn (Yuanzhuo Geng)
[1]PhD Student, Dept. of Control Science and Engineering, Harbin Institute of Technology.
[2]Professor, Dept. of Control Science and Engineering, Harbin Institute of Technology.
[3]Associate Professor, Dept. of Control Science and Engineering, Harbin Institute of Technology.
[4]Associate Professor, Dept. of Aerospace Science and Technology, Politecnico di Milano.

proved SDRE approach combined with a waypoint is proposed to enhance control performance. Finally, numerical investigations are conducted and compared with the real optimal solutions obtained by using the optimization software.
Keywords:
Repointing maneuver, Fixed-time optimal control, SDRE method, Waypoint

1. Introduction

There is an increasing demand for many space-based applications to continuously observe an area of the Earth with high resolution for a prescribed time [1, 2]. Such observations are essential for military reconnaissance, environmental monitoring, disaster prevention, and border security. The real-time staring mode [3], with the optical axis fixed to the target, proves to be a more effective solution compared with push-broom TDI-CCD imaging, as it can provide dynamic observations such as with a video satellite whereby no scanning mechanisms are required [4]. Different from most attitude reorientation problems, staring-mode observations only require that the optical axis of the area-array camera points to the target. In this case no constraints on the rotation around the optical axis are necessary. Hence, the final attitude is constrained within a given set which is defined by nonlinear constraints rather than a fixed pointing vector. These relaxed constraints (when compared to fixed point constraints) provide more flexibility for attitude slew planning. In recent years, staring-mode observations have been performed by satellites such as LAPAN-Tubsat, GF-4, and Jilin No. 1. Mission planning and attitude control of a single satellite for multi-object staring imaging has been investigated in [5–7], respectively.

Here, the spacecraft is required to repoint the optical axis from an initial posi-

tion vector to a desired target axis while minimizing the energy on the spacecraft which enhances the control efficiency. In this paper the repointing maneuver is formulated as a fixed-time optimal control problem with nonlinear terminal constraints and solved by using finite-time horizon dynamic optimization theory.

Nonlinear optimal control such as the pseudo-spectral method has been widely used for attitude control design [8–11]. However pseudo-spectral methods can only provide open-loop solutions numerically and are susceptible to initial conditions, external disturbances, and internal uncertainties such as variations in mass and the inertia matrix due to fuel usage or sloshing. A closed-loop optimal control scheme was established using dynamic programming in which sufficient conditions for the optimality were given and that is robust to uncertainties in the system [12]. However, the Hamilton-Jacobi-Bellman(HJB) equation in dynamic programming is difficult to be solved[13–15], which limits the applications of these methods for practical engineering problems, such as the spacecraft repointing problem posed here.

An alternative approach to solve nonlinear optimal control problems is the state-dependent Riccati equation (SDRE) control synthesis which dates back to 1962 [16]. The SDRE method entails factorization of the nonlinear dynamics into the product of a state-dependent matrix and the state vector thereby transforming the original nonlinear system into a pseudo-linear system [17–21]. In [22], a real-time LQR-based suboptimal approach for full six degree-of-freedom spacecraft control was proposed. Xu [23] applied the SDRE method to the motion and attitude control of spacecraft approaching a tumbling target.

These advancements in the SDRE method have only previously considered closed-loop infinite-horizon optimal control problems. However, the time re-

quired for tasking and slewing is limited in the context of staring-mode observation. In [24], a finite-time control scheme based on a finite-time disturbance observer was created for trajectory tracking of a surface vehicle. In [25] and [26], the finite-time horizon SDRE method was introduced to control both nonlinear time-varying non-affine and affine systems. Ali [27] provided an approximate closed-form solution to the finite-horizon optimal control problem and applied the technique to path-planning of a reusable launch vehicle. In addition, the local convergence properties of the closed-loop system were analyzed in [28]. Although these methods can cope with terminal point constraints, they are not readily applicable to terminal constraint sets. Moreover, with terminal constraint sets the final states are not precisely known, thus the value of the gain matrices which need to be calculated at each time-step using backward integration of this final condition is not possible.

To handle the optimal control problem with linear terminal constraint sets, the sweep method was developed [29]. Vadali [30] proposed a power-series solution methodology to design the finite-time feedback controller for the nonlinear systems with nonlinear terminal constraints in which the cost-to-go function is approximated by a polynomial series involving states and terminal Lagrange multipliers. However, the generation of the equations for gain coefficients is a computationally expensive process. Recently, Sharma [31] formulated a near-optimal control approach and used SDRE to demonstrate through simulation that it can provide a practical solution for closed-loop control. Although this near-optimal control approach is valuable in practice, the stability analysis necessary to guarantee that the approach always works was not established. This paper extends this analysis by providing a more efficient solution to this near-optimal control

approach while providing the stability and convergence guarantees necessary for practical implementation.

Inspired by the above discussion, the motivations of our paper involve two aspects. The first one is to deal with the nonlinear optimal control problem with a nonlinear terminal constraint set that has rarely been studied and thus it is still an open problem to be addressed as mentioned in [29–31]. The other motivation is to improve the control performance of the traditional SDRE method. For the traditional SDRE method proposed in [31], the control performance gets seriously bad for strong nonlinear systems such as large angle repointing maneuvers of the spacecraft. An improved SDRE approach is to be proposed in this paper to overcome the inherent deficiencies in the traditional SDRE method and enhance computation efficiency.

The main contributions of this paper are as follows:

(1) A new description for repointing maneuver is presented in which the final desired attitude is described as a nonlinear constraint instead of a fixed point.

(2) The fixed-time optimal repointing maneuver problem is successfully resolved based on SDRE dynamic programming method. A simple yet efficient way of handling the nonlinear terminal constraints are presented. Besides, a rigorous stability analysis for the closed-loop system is given in which the convergence for the spacecraft attitude control system from the initial attitude to the final attitude constraint is guaranteed. As far as we know, it is the first time that the stability of the system with a nonlinear terminal constraint is proved.

(3) Considering the inherent deficiency of the SDRE method that the control performance degrades seriously for large angle maneuvers, a novel waypoint method is presented and combined with the SDRE approach, in which the whole

time interval is partitioned into two segments. Compared with the traditional S-DRE method in [31], the improved SDRE approach could enhance the control performance and optimality for the system, especially for the large angle maneuvers. Moreover, from a practical point of view, the waypoint method could reduce the computation burden involved in the SDRE method thus it is more efficient to implement on board.

This paper is organized as follows: Section2 describes the optimal control problem for repointing maneuver of the rigid spacecraft, and the boundary conditions of the final required attitude sets are given. Section 3 establishes the SDRE based nonlinear optimal control scheme, allowing exact pointing of the body-fixed optic axis toward an arbitrary orientation in inertial space with the minimum cost. The waypoint method is introduced thereafter. Section 4 illustrates the validity of the presented approach through numerical simulations, followed by conclusions in Section 5.

2. Problem formulation

2.1. Spacecraft model description

The rotation dynamics of the rigid spacecraft can be described as

$$\dot{\bar{\boldsymbol{q}}} = \frac{1}{2}\Xi(\boldsymbol{q})\boldsymbol{\omega} = \frac{1}{2}\begin{bmatrix} q_4\boldsymbol{I} + \boldsymbol{q}^{\times} \\ -\boldsymbol{q}^{\mathrm{T}} \end{bmatrix}\boldsymbol{\omega} \tag{1}$$

$$\dot{\boldsymbol{\omega}} = -\boldsymbol{J}_{\mathrm{s}}^{-1}\boldsymbol{\omega}^{\times}\boldsymbol{J}_{\mathrm{s}}\boldsymbol{\omega} + \boldsymbol{J}_{\mathrm{s}}^{-1}\boldsymbol{u} \tag{2}$$

where $\bar{\boldsymbol{q}}$ is the attitude quaternion with respect to inertial space and it consists of the vector part $\boldsymbol{q} = [q_1\ q_2\ q_3]^{\mathrm{T}}$ and the scalar part q_4. $\boldsymbol{\omega}$ is the vector of angular

velocities in body axis coordinates, $\boldsymbol{u}$ represents the control torque, $\boldsymbol{J}_{\mathrm{s}}$ is the inertia matrix. We use $\boldsymbol{a}^{\times}$ to denote the skew-symmetric matrix

$$\boldsymbol{a}^{\times} = \begin{bmatrix} 0 & -a_3 & a_2 \\ a_3 & 0 & -a_1 \\ -a_2 & a_1 & 0 \end{bmatrix} \tag{3}$$

where $\boldsymbol{a} = [a_1\ a_2\ a_3]^{\mathrm{T}}$.

The rotation dynamics of the rigid spacecraft Eqs.(1) and (2) can be expressed in a pseudo-linear form as

$$\dot{\boldsymbol{x}} = \boldsymbol{f}(\boldsymbol{x}, \boldsymbol{u}) = \boldsymbol{A}(\boldsymbol{x}) + \boldsymbol{B}(\boldsymbol{x})\boldsymbol{u} \tag{4}$$

where $\boldsymbol{x} = [q_1, q_2, q_3, q_4, \omega_1, \omega_2, \omega_3]^{\mathrm{T}}$, $\boldsymbol{A}(\boldsymbol{x}) = \begin{bmatrix} \boldsymbol{0}_{4\times4} & \boldsymbol{A}_1(\boldsymbol{x}) \\ \boldsymbol{0}_{3\times4} & \boldsymbol{A}_2(\boldsymbol{x}), \end{bmatrix}$, $\boldsymbol{B}(\boldsymbol{x}) = \begin{bmatrix} \boldsymbol{0}_{4\times3} \\ \boldsymbol{J}_{\mathrm{s}}^{-1} \end{bmatrix}$, $\boldsymbol{A}_1(\boldsymbol{x}) = \frac{1}{2}\begin{bmatrix} q_4\boldsymbol{I} + \boldsymbol{q}^{\times} \\ -\boldsymbol{q}^T \end{bmatrix}$, $\boldsymbol{A}_2(\boldsymbol{x}) = -\boldsymbol{J}_{\mathrm{s}}^{-1}\boldsymbol{\omega}^{\times}\boldsymbol{J}_{\mathrm{s}}$. $\boldsymbol{A}(\boldsymbol{x})$ and $\boldsymbol{B}(\boldsymbol{x})$ are State-Dependent Coefficient (SDC) matrices.

Remark 1. Although the construction of the SDC matrices for Eq.(4) is not unique, the pointwise controllability of the pair $(\boldsymbol{A}(\boldsymbol{x}), \boldsymbol{B}(\boldsymbol{x}))$ and the observability of the pair $(\boldsymbol{A}(\boldsymbol{x}), \boldsymbol{Q}^{\frac{1}{2}})$ need to be satisfied[19].

For simplicity, arguments of $\boldsymbol{A}(\boldsymbol{x})$ and $\boldsymbol{B}(\boldsymbol{x})$ are dropped in the following sections.

2.2. Boundary conditions

In this subsection, the initial and final conditions for repointing maneuver of the spacecraft with both zero and nonzero final angular velocities are given. For a

specific target orientation, the nonlinear terminal constraints are to be established in terms of quaternion parameters and angular velocities of the spacecraft.

Without loss of generality, the initial attitude is considered to be

$$\boldsymbol{x}_{t_0} = [q_{10}, q_{20}, q_{30}, q_{40}, \omega_{10}, \omega_{20}, \omega_{30}]^{\mathrm{T}} \tag{5}$$

However, the final quaternion $\boldsymbol{q}_{t_\mathrm{f}}$ is unknown because the rotation about the optic axis X_b is free. In other words, the final rotation angle about the optic axis is also a variable to be optimized.

The direction-cosine matrix between the body frame and the reference(inertial) frame is expressed in terms of quaternion parameters as

$$\boldsymbol{R}_{br} = \begin{bmatrix} q_1^2 - q_2^2 - q_3^2 + q_4^2 & 2(q_1q_2 + q_3q_4) & 2(q_1q_3 - q_2q_4) \\ 2(q_1q_2 - q_3q_4) & -q_1^2 + q_2^2 - q_3^2 + q_4^2 & 2(q_2q_3 + q_1q_4) \\ 2(q_1q_3 + q_2q_4) & 2(q_2q_3 - q_1q_4) & -q_1^2 - q_2^2 + q_3^2 + q_4^2 \end{bmatrix} \tag{6}$$

Let $\boldsymbol{t}^\mathrm{b}$ and $\boldsymbol{t}^\mathrm{i}$ represent the coordinate of the target orientation $\boldsymbol{t}$ expressed in the body-fixed frame and in the inertial frame, respectively. The relation between $\boldsymbol{t}^\mathrm{b}$ and $\boldsymbol{t}^\mathrm{i}$ is $\boldsymbol{t}^\mathrm{b} = \boldsymbol{R}_{br}\boldsymbol{t}^\mathrm{i}$. The optic axis X_b should be aligned with the target orientation $\boldsymbol{t}$ in the end, namely

$$\boldsymbol{t}^\mathrm{b} = \boldsymbol{R}_{br}\boldsymbol{t}^\mathrm{i} = [1\ 0\ 0]^{\mathrm{T}} \tag{7}$$

The terminal quaternion equations can be derived from Eqs. (6)and (7) as

$$(q_{1\mathrm{f}}^2 - q_{2\mathrm{f}}^2 - q_{3\mathrm{f}}^2 + q_{4\mathrm{f}}^2)t_x^\mathrm{i} + 2(q_{1\mathrm{f}}q_{2\mathrm{f}} + q_{3\mathrm{f}}q_{4\mathrm{f}})t_y^\mathrm{i} + 2(q_{1\mathrm{f}}q_{3\mathrm{f}} - q_{2\mathrm{f}}q_{4\mathrm{f}})t_z^\mathrm{i} = 1 \tag{8}$$

$$2(q_{1\mathrm{f}}q_{2\mathrm{f}} - q_{3\mathrm{f}}q_{4\mathrm{f}})t_x^\mathrm{i} + (-q_{1\mathrm{f}}^2 + q_{2\mathrm{f}}^2 - q_{3\mathrm{f}}^2 + q_{4\mathrm{f}}^2)t_y^\mathrm{i} + 2(q_{2\mathrm{f}}q_{3\mathrm{f}} + q_{1\mathrm{f}}q_{4\mathrm{f}})t_z^\mathrm{i} = 0 \tag{9}$$

$$2(q_{1\mathrm{f}}q_{3\mathrm{f}} + q_{2\mathrm{f}}q_{4\mathrm{f}})t_x^\mathrm{i} + 2(q_{2\mathrm{f}}q_{3\mathrm{f}} - q_{1\mathrm{f}}q_{4\mathrm{f}})t_y^\mathrm{i} + (-q_{1\mathrm{f}}^2 - q_{2\mathrm{f}}^2 + q_{3\mathrm{f}}^2 + q_{4\mathrm{f}}^2)t_z^\mathrm{i} = 0 \tag{10}$$

where $q_{1\mathrm{f}}$, $q_{2\mathrm{f}}$, $q_{3\mathrm{f}}$, and $q_{4\mathrm{f}}$ are terminal quaternion components and t_x^{i}, t_y^{i}, and t_z^{i} are expressions of the target orientation in the inertial frame. In fact, the terminal attitude constraints expressed in Eqs.(8), (9) and (10) are redundant. The Eq.(8) implies that the X_{b} axis is aligned with the target orientation $\boldsymbol{t}$ in the end, while Eqs. (9)and (10) mean that the $\boldsymbol{t}$ is perpendicular to Y_{b} and Z_{b} respectively. Obviously, if Eq.(8) is satisfied, then Eqs.(9) and (10) are automatically satisfied. Therefore, only Eq.(8) is required for terminal quaternion constraints description.

In some circumstances, such as moving targets detection and Earth observation, the final angular velocities are required to be non-zero. Although the desired final angular velocity in the inertial frame of the spacecraft denoted by $\boldsymbol{\omega}_{\mathrm{f}}^{\mathrm{i}}$ can be determined according to the targets speed, it cannot be directly expressed in the body frame due to the unspecific terminal body attitude. Thus, to construct terminal angular velocity constraint in the body frame, the coordinates transformation is required that

$$\boldsymbol{\omega}_{\mathrm{f}}^{\mathrm{b}} = \boldsymbol{R}_{br}\boldsymbol{\omega}_{\mathrm{f}}^{\mathrm{i}} \tag{11}$$

where $\boldsymbol{\omega}_{\mathrm{f}}^{\mathrm{b}}$ is the terminal angular velocity expressed in the body frame.

Then the terminal constraints of the spacecraft working in staring-mode for

moving target detection are established via Eqs.(8) and (11) as

$$\begin{aligned}
\psi_1(\boldsymbol{x}_{t_\mathrm{f}}) &= (q_{1\mathrm{f}}^2 - q_{2\mathrm{f}}^2 - q_{3\mathrm{f}}^2 + q_{4\mathrm{f}}^2)t_{x\mathrm{f}}^{\mathrm{i}} + 2(q_{1\mathrm{f}}q_{2\mathrm{f}} + q_{3\mathrm{f}}q_{4\mathrm{f}})t_{y\mathrm{f}}^{\mathrm{i}} \\
&\quad +2(q_{1\mathrm{f}}q_{3\mathrm{f}} - q_{2\mathrm{f}}q_{4\mathrm{f}})t_{z\mathrm{f}}^{\mathrm{i}} = 1 \\
\psi_2(\boldsymbol{x}_{t_\mathrm{f}}) &= (q_{1\mathrm{f}}^2 - q_{2\mathrm{f}}^2 - q_{3\mathrm{f}}^2 + q_{4\mathrm{f}}^2)\omega_{1\mathrm{f}}^{\mathrm{i}} + 2(q_{1\mathrm{f}}q_{2\mathrm{f}} + q_{3\mathrm{f}}q_{4\mathrm{f}})\omega_{2\mathrm{f}}^{\mathrm{i}} \\
&\quad +2(q_{1\mathrm{f}}q_{3\mathrm{f}} - q_{2\mathrm{f}}q_{4\mathrm{f}})\omega_{3\mathrm{f}}^{\mathrm{i}} - \omega_{1\mathrm{f}}^{\mathrm{b}} = 0 \\
\psi_3(\boldsymbol{x}_{t_\mathrm{f}}) &= 2(q_{1\mathrm{f}}q_{2\mathrm{f}} - q_{3\mathrm{f}}q_{4\mathrm{f}})\omega_{1\mathrm{f}}^{\mathrm{i}} + (-q_{1\mathrm{f}}^2 + q_{2\mathrm{f}}^2 - q_{3\mathrm{f}}^2 + q_{4\mathrm{f}}^2)\omega_{2\mathrm{f}}^{\mathrm{i}} \\
&\quad +2(q_{2\mathrm{f}}q_{3\mathrm{f}} + q_{1\mathrm{f}}q_{4\mathrm{f}})\omega_{3\mathrm{f}}^{\mathrm{i}} - \omega_{2\mathrm{f}}^{\mathrm{b}} = 0 \\
\psi_4(\boldsymbol{x}_{t_\mathrm{f}}) &= 2(q_{1\mathrm{f}}q_{3\mathrm{f}} + q_{2\mathrm{f}}q_{4\mathrm{f}})\omega_{1\mathrm{f}}^{\mathrm{i}} + 2(q_{2\mathrm{f}}q_{3\mathrm{f}} - q_{1\mathrm{f}}q_{4\mathrm{f}})\omega_{2\mathrm{f}}^{\mathrm{i}} \\
&\quad +(-q_{1\mathrm{f}}^2 - q_{2\mathrm{f}}^2 + q_{3\mathrm{f}}^2 + q_{4\mathrm{f}}^2)\omega_{3\mathrm{f}}^{\mathrm{i}} - \omega_{3\mathrm{f}}^{\mathrm{b}} = 0
\end{aligned} \tag{12}$$

where $\psi_1(\boldsymbol{x}_{t_\mathrm{f}})$, $\psi_2(\boldsymbol{x}_{t_\mathrm{f}})$, $\psi_3(\boldsymbol{x}_{t_\mathrm{f}})$, and $\psi_4(\boldsymbol{x}_{t_\mathrm{f}})$ are nonlinear equations with respect to the terminal quaternion parameters $q_{1\mathrm{f}}$, $q_{2\mathrm{f}}$, $q_{3\mathrm{f}}$, $q_{4\mathrm{f}}$ and terminal angular velocity components $\omega_{1\mathrm{f}}^{\mathrm{b}}$, $\omega_{2\mathrm{f}}^{\mathrm{b}}$ and $\omega_{3\mathrm{f}}^{\mathrm{b}}$ for a specific target orientation $\boldsymbol{t}^{\mathrm{i}}$ and a desired terminal angular velocity $\boldsymbol{\omega}_{\mathrm{f}}^{\mathrm{i}}$. $t_{x\mathrm{f}}^{\mathrm{i}}$, $t_{y\mathrm{f}}^{\mathrm{i}}$, $t_{z\mathrm{f}}^{\mathrm{i}}$ means the final target orientation at $t = t_\mathrm{f}$. The nonlinear equation Eq.(12) is underdetermined thus given a target orientation $\boldsymbol{t}^{\mathrm{i}}$ the solution of terminal attitude $q_{1\mathrm{f}}$, $q_{2\mathrm{f}}$, $q_{3\mathrm{f}}$, $q_{4\mathrm{f}}$ is not unique. Note that for classical three-axis attitude reorientation, the final desired attitude is explicitly known. Thus the value of $q_{1\mathrm{f}}$, $q_{2\mathrm{f}}$, $q_{3\mathrm{f}}$, $q_{4\mathrm{f}}$, $\omega_{1\mathrm{f}}^{\mathrm{b}}$, $\omega_{2\mathrm{f}}^{\mathrm{b}}$, and $\omega_{3\mathrm{f}}^{\mathrm{b}}$ can be obtained easily. But for repointing maneuver, they form a group of underdetermined equations. For simplicity, terminal constraints of Eq.(12) can be presented in a vector form as $\boldsymbol{\psi}(\boldsymbol{x}(t_\mathrm{f})) = \boldsymbol{\psi}_\mathrm{f} \in \mathbb{R}^{4\times 1}$ and $\boldsymbol{\psi}_\mathrm{f} = [1\ 0\ 0\ 0]^{\mathrm{T}}$ here.

*2.3. **Description of the optimal control problem***

The finite-horizon optimal control problem for repointing maneuver is to find a control sequence which drives the spacecraft from its initial attitude $\boldsymbol{x}(t_0)$ to its final attitude $\boldsymbol{x}(t_\mathrm{f})$ expressed by Eqs.(5) and (12) for the system of Eq.(4) at a final

time t_f , while minimizing the cost function

$$J = \phi(\boldsymbol{x}(t_\mathrm{f})) + \frac{1}{2}\int_{t_0}^{t_\mathrm{f}} (\boldsymbol{x}^\mathrm{T}\boldsymbol{Q}\boldsymbol{x} + \boldsymbol{u}^\mathrm{T}\boldsymbol{R}\boldsymbol{u})\, d\tau \tag{13}$$

where $\boldsymbol{Q} \geqslant 0$ and $\boldsymbol{R} > 0$ are constant weight matrices. $\phi(\boldsymbol{x}(t_\mathrm{f}))$ can be viewed as the soft constraint that is ignored in this paper.

$\boldsymbol{x}^\mathrm{T}\boldsymbol{Q}\boldsymbol{x}$ in Eq.(13) consists of a quadratic form with respect to the quaternion and the angular velocity. In fact, the integration of the quaternion makes no sense. But interestingly, the quadratic sum of the elements of the quaternion is a constant if they have the same coefficients of $\boldsymbol{Q}$. Thus the quaternion related term has no effect on optimization solutions. The full-rank matrix $\boldsymbol{Q}$ is only to satisfy the requirement for the observability of the pair $\left(\boldsymbol{A}(\boldsymbol{x}), \boldsymbol{Q}^{\frac{1}{2}}\right)$.

3. SDRE-based near optimal controller design

In this section, the nonlinear terminal constraints of Eq.(12) are tackled by successive linearization method first and then the finite-time horizon optimal controller is designed based on the traditional SDRE method and the waypoint-based SDRE approach, respectively.

3.1. Linearization of nonlinear terminal constraints

In previous work [29, 30], no effective way of handling the nonlinear terminal constraints of Eq.(12) using the dynamic programming method has been given. In this paper a successive linearization method is adopted in which the nonlinear equations in Eq.(12) are linearized at each step by use of the first-order Taylor expansion at the current state $\boldsymbol{x}(t)$ as follows[31].

$$\boldsymbol{\psi}(\boldsymbol{x}(t_\mathrm{f})) = \boldsymbol{\psi}(\boldsymbol{x}(t)) + \boldsymbol{\psi}_{\boldsymbol{x}|\boldsymbol{x}_t}(\boldsymbol{x}(t_\mathrm{f}) - \boldsymbol{x}(t)) = \boldsymbol{\psi}_\mathrm{f} \tag{14}$$

in which $\boldsymbol{\psi}_{\boldsymbol{x}|\boldsymbol{x}_t}$ is the Jacobian matrix evaluated at the current sate $\boldsymbol{x}(t)$. Then the pointwise pseudo-linear terminal constraints can be derived from Eq.(14) as

$$\boldsymbol{\psi}(\boldsymbol{x}(t_{\mathrm{f}})) = \bar{\boldsymbol{C}}\boldsymbol{x}(t_{\mathrm{f}}) = \bar{\boldsymbol{\psi}}_{\mathrm{f}} \tag{15}$$

where $\bar{\boldsymbol{C}} = \boldsymbol{\psi}_{\boldsymbol{x}|\boldsymbol{x}_t}$, $\bar{\boldsymbol{\psi}}_{\mathrm{f}} = \boldsymbol{\psi}_{\mathrm{f}} + \boldsymbol{\psi}_{\boldsymbol{x}|\boldsymbol{x}_t}\boldsymbol{x}(t) - \boldsymbol{\psi}(\boldsymbol{x}(t))$. Obviously, $\bar{\boldsymbol{C}}$ and $\bar{\boldsymbol{\psi}}_{\mathrm{f}}$ are state-dependent matrices.

*3.2. **Finite-time horizon near-optimal controller design***

Based on the HJB theory, we formulate the HJB equation as follows:

$$-\frac{\partial J^*(\boldsymbol{x},t)}{\partial t} = H(\boldsymbol{x},\boldsymbol{u}^*,\boldsymbol{\lambda}^*,t) = \frac{1}{2}(\boldsymbol{x}^T\boldsymbol{Q}\boldsymbol{x} + \boldsymbol{u}^T\boldsymbol{R}\boldsymbol{u}) + \boldsymbol{\lambda}^{*\mathrm{T}}(\boldsymbol{A}\boldsymbol{x} + \boldsymbol{B}\boldsymbol{u}) \tag{16}$$

where $J^*(\boldsymbol{x},t)$ is the optimal cost-to-go function defined as

$$J^*(\boldsymbol{x},t) = \inf_{\boldsymbol{u}} \frac{1}{2}\int_{t_0}^{t_{\mathrm{f}}} (\boldsymbol{x}^{\mathrm{T}}\boldsymbol{Q}\boldsymbol{x} + \boldsymbol{u}^{\mathrm{T}}\boldsymbol{R}\boldsymbol{u})\, d\tau \tag{17}$$

with the boundary condition

$$J^*((\boldsymbol{x}(t_{\mathrm{f}})), t_{\mathrm{f}}) = \phi(\boldsymbol{x}(t_{\mathrm{f}})) = 0 \tag{18}$$

$H(\boldsymbol{x},\boldsymbol{u}^*,\boldsymbol{\lambda}^*,t)$ is the Hamiltonian for the problem, and $\boldsymbol{\lambda}^*$ is the costate vector that holds

$$\boldsymbol{\lambda}^* = \frac{\partial J^*(\boldsymbol{x},t)}{\partial \boldsymbol{x}} \tag{19}$$

According to the Pontryagins minimum principle, the optimal control can be derived in the following form

$$\boldsymbol{u}^* = -\boldsymbol{R}^{-1}\boldsymbol{B}^{\mathrm{T}}\frac{\partial J^*(\boldsymbol{x},t)}{\partial \boldsymbol{x}} \tag{20}$$

The transversality condition is

$$\boldsymbol{\lambda}(t_{\mathrm{f}}) = \frac{\partial \phi}{\partial \boldsymbol{x}(t_{\mathrm{f}})} + \frac{\partial \boldsymbol{\psi}^{\mathrm{T}}}{\partial \boldsymbol{x}(t_{\mathrm{f}})}\boldsymbol{\nu} \tag{21}$$

where $\boldsymbol{\nu} \in \mathbb{R}^{4\times 1}$ is the terminal Lagrange multiplier to guarantee that the system satisfies the terminal constraints.

The centerpiece of dynamic programming is to determine the optimal cost-to-go function $J^*(\boldsymbol{x}, t)$ that is extremely difficult to be solved[32, 33]. The SDRE-based method rebuilds the nonlinear spacecraft attitude control system in terms of the pseudo-linear form and thus the LQR theory can be used to design the optimal controller. Motivated by the linear optimal control theory, $J^*(\boldsymbol{x}, t)$ is estimated as

$$\hat{J}^* = \frac{1}{2}\boldsymbol{x}^{\mathrm{T}}\boldsymbol{S}_0(t)\boldsymbol{x} + \frac{1}{2}\boldsymbol{\nu}^{\mathrm{T}}\boldsymbol{V}_0(t)\boldsymbol{\nu} + \boldsymbol{\nu}^{\mathrm{T}}\boldsymbol{P}_0(t)\boldsymbol{x} + \boldsymbol{S}_1^{\mathrm{T}}(t)\boldsymbol{x} + \boldsymbol{V}_1^{\mathrm{T}}(t)\boldsymbol{\nu} + P_1(t) \tag{22}$$

where $\boldsymbol{S}_0$, $\boldsymbol{V}_0$, $\boldsymbol{P}_0$, $\boldsymbol{S}_1$, $\boldsymbol{V}_1$and P_1 are time-varying gain matrices. Note that $\boldsymbol{S}_0$ can be assumed to be a symmetric positive definite matrix while $\boldsymbol{V}_0$ is a symmetric and negative definite matrix. The controller can be calculated from Eqs.(20) and (22)

$$\boldsymbol{u}^* = -\boldsymbol{R}^{-1}\boldsymbol{B}^{\mathrm{T}}\frac{\partial J^*(\boldsymbol{x}, t)}{\partial \boldsymbol{x}} = -\boldsymbol{R}^{-1}\boldsymbol{B}^{\mathrm{T}}(\boldsymbol{S}_0\boldsymbol{x} + \boldsymbol{P}_0^{\mathrm{T}}\boldsymbol{\nu} + \boldsymbol{S}_1) \tag{23}$$

Furthermore, according to [30], the terminal Lagrange multiplier should follow

$$\frac{\partial \hat{J}^*}{\partial \boldsymbol{\nu}} = \boldsymbol{0} \tag{24}$$

Then $\boldsymbol{\nu}$ can be obtained by applying Eq.(22) to Eq.(24), which yields

$$\boldsymbol{\nu} = -{\boldsymbol{V}_0}^{-1}(\boldsymbol{P}_0\boldsymbol{x} + \boldsymbol{V}_1) \tag{25}$$

The next step is to determine the time-varying gain matrices of $\hat{J}^*$ in Eq.(22).

Substituting Eqs.(19), (22) and (23) into Eq.(16) with some combinations, the HJB equation can be written as

$$\begin{aligned} -\tfrac{\partial \hat{J}^*(\boldsymbol{x},t)}{\partial t} &= -\tfrac{1}{2}\boldsymbol{x}^{\mathrm{T}}\dot{\boldsymbol{S}}_0(t)\boldsymbol{x} - \tfrac{1}{2}\boldsymbol{\nu}^{\mathrm{T}}\dot{\boldsymbol{V}}_0(t)\boldsymbol{\nu} - \boldsymbol{\nu}^{\mathrm{T}}\dot{\boldsymbol{P}}_0(t)\boldsymbol{x} - \boldsymbol{x}^{\mathrm{T}}\dot{\boldsymbol{S}}_1(t) - \boldsymbol{\nu}^{\mathrm{T}}\dot{\boldsymbol{V}}_1(t) - \dot{P}_1(t) \\ &= \tfrac{1}{2}\boldsymbol{x}^{\mathrm{T}}(\boldsymbol{Q} - \boldsymbol{S}_0\boldsymbol{B}\boldsymbol{R}^{-1}\boldsymbol{B}^{\mathrm{T}}\boldsymbol{S}_0 + \boldsymbol{S}_0\boldsymbol{A} + \boldsymbol{A}^{\mathrm{T}}\boldsymbol{S}_0)\boldsymbol{x} - \tfrac{1}{2}\boldsymbol{\nu}^{\mathrm{T}}\boldsymbol{P}_0\boldsymbol{B}\boldsymbol{R}^{-1}\boldsymbol{B}^{\mathrm{T}}\boldsymbol{P}_0^{\mathrm{T}}\boldsymbol{\nu} \\ &\quad +\boldsymbol{\nu}^{\mathrm{T}}(-\boldsymbol{P}_0\boldsymbol{B}\boldsymbol{R}^{-1}\boldsymbol{B}^{\mathrm{T}}\boldsymbol{S}_0 + \boldsymbol{P}_0\boldsymbol{A})\boldsymbol{x} + \boldsymbol{x}^{\mathrm{T}}(-\boldsymbol{S}_0^{\mathrm{T}}\boldsymbol{B}\boldsymbol{R}^{-1}\boldsymbol{B}^{\mathrm{T}}\boldsymbol{S}_1 + \boldsymbol{A}^{\mathrm{T}}\boldsymbol{S}_1) \\ &\quad +\boldsymbol{\nu}^{\mathrm{T}}(-\boldsymbol{P}_0\boldsymbol{B}\boldsymbol{R}^{-1}\boldsymbol{B}^{\mathrm{T}}\boldsymbol{S}_1) - \tfrac{1}{2}\boldsymbol{S}_1^{\mathrm{T}}\boldsymbol{B}\boldsymbol{R}^{-1}\boldsymbol{B}^{\mathrm{T}}\boldsymbol{S}_1 \end{aligned} \tag{26}$$

Then the time-varying gain matrices can be calculated as

$$\begin{aligned} \dot{\boldsymbol{S}}_0 &= -(\boldsymbol{Q} - \boldsymbol{S}_0\boldsymbol{B}\boldsymbol{R}^{-1}\boldsymbol{B}^{\mathrm{T}}\boldsymbol{S}_0 + \boldsymbol{S}_0\boldsymbol{A} + \boldsymbol{A}^{\mathrm{T}}\boldsymbol{S}_0) \\ \dot{\boldsymbol{V}}_0 &= \boldsymbol{P}_0\boldsymbol{B}\boldsymbol{R}^{-1}\boldsymbol{B}^{\mathrm{T}}\boldsymbol{P}_0^{\mathrm{T}} \\ \dot{\boldsymbol{P}}_0 &= -(-\boldsymbol{P}_0\boldsymbol{B}\boldsymbol{R}^{-1}\boldsymbol{B}^{\mathrm{T}}\boldsymbol{S}_0 + \boldsymbol{P}_0\boldsymbol{A}) \\ \dot{\boldsymbol{S}}_1 &= -(-\boldsymbol{S}_0^{\mathrm{T}}\boldsymbol{B}\boldsymbol{R}^{-1}\boldsymbol{B}^{\mathrm{T}}\boldsymbol{S}_1 + \boldsymbol{A}^{\mathrm{T}}\boldsymbol{S}_1) \\ \dot{\boldsymbol{V}}_1 &= \boldsymbol{P}_0\boldsymbol{B}\boldsymbol{R}^{-1}\boldsymbol{B}^{\mathrm{T}}\boldsymbol{S}_1 \\ \dot{P}_1 &= \tfrac{1}{2}\boldsymbol{S}_1^{\mathrm{T}}\boldsymbol{B}\boldsymbol{R}^{-1}\boldsymbol{B}^{\mathrm{T}}\boldsymbol{S}_1 \end{aligned} \tag{27}$$

The derivatives of these gain matrices form a group differential equations that need to be solved for control law design. To obtain the value of the gain matrices at each time-step, the boundary conditions at t_{f} need to be given. Using Eq.(21), along with Eqs.(19) and (22), the equation

$$\boldsymbol{S}_0(t_{\mathrm{f}})\boldsymbol{x}(t_{\mathrm{f}}) + \boldsymbol{P}_0^{\mathrm{T}}(t_{\mathrm{f}})\boldsymbol{\nu} + \boldsymbol{S}_1(t_{\mathrm{f}}) = \frac{\partial \phi}{\partial \boldsymbol{x}(t_{\mathrm{f}})} + \bar{\boldsymbol{C}}^{\mathrm{T}}\boldsymbol{\nu} \tag{28}$$

is generated and then the terminal value of $\boldsymbol{S}_0$, $\boldsymbol{P}_0$ and $\boldsymbol{S}_1$ can be derived as

$$\boldsymbol{S}_0(t_{\mathrm{f}}) = \boldsymbol{0},\ \boldsymbol{S}_1(t_{\mathrm{f}}) = \boldsymbol{0},\ \boldsymbol{P}_0(t_{\mathrm{f}}) = \bar{\boldsymbol{C}} \tag{29}$$

under the assumption that ϕ in Eq.(13) is zero. Besides, substituting Eq.(22) into Eq.(24) yields

$$\boldsymbol{V}_0(t_{\mathrm{f}})\boldsymbol{\nu} + \boldsymbol{P}_0(t_{\mathrm{f}})\boldsymbol{x}(t_{\mathrm{f}}) + \boldsymbol{V}_1(t_{\mathrm{f}}) = \boldsymbol{0} \tag{30}$$

Recalling $\bar{\boldsymbol{C}}\boldsymbol{x}(t_\mathrm{f}) = \bar{\boldsymbol{\psi}}_\mathrm{f}$ and $\boldsymbol{P}_0(t_\mathrm{f}) = \bar{\boldsymbol{C}}$ as shown in Eqs.(15) and (29), one can obtain that

$$\boldsymbol{V}_0(t_\mathrm{f}) = \boldsymbol{0},\ \boldsymbol{V}_1(t_\mathrm{f}) = -\bar{\boldsymbol{\psi}}_\mathrm{f} \tag{31}$$

Consequently, according to the boundary condition of $\hat{J}^*$ given in Eq.(18), the $P_1(t_\mathrm{f})$ can be obtained as

$$P_1(t_\mathrm{f}) = 0 \tag{32}$$

Ultimately, the time-varying gain matrices of $\hat{J}^*$ at each time step can be calculated via Eq.(27) with the boundary conditions shown in Eqs.(29), (31) and (32) by backward integration from t_f to t. It should be noted that there is a problem in solving Eq.(27) with the boundary conditions because the differential equations in Eq.(27) involve the state-dependent matrix $\boldsymbol{A}$ that is not known ahead of time. To remedy the problem, the values of the states in Eq.(27) are frozen at their current values from the current time to the final time at each step[28]. The control accuracy and optimality is lost for this approximation method to some extent.

Remark 2. The terminal Lagrange multiplier $\boldsymbol{\nu}$ updated by using Eq.(25) becomes singular at the final time t_f. Hence, the simulation is ought to be stopped before the final time.

Remark 3. In fact, the gain matrices $\boldsymbol{S}_1$ and $\boldsymbol{P}_1$ are both zero as we can see from Eq.(27) that the derivatives of $\boldsymbol{S}_1$ and $\boldsymbol{P}_1$ are zero if $P_1(t_\mathrm{f}) = 0$ and $\boldsymbol{S}_1(t_\mathrm{f}) = \boldsymbol{0}$.

*3.3. **Stability analysis***

Generally, the stability is paramount for spacecraft because it can guarantee that the states converge to the equilibrium point and stay around it under disturbances and uncertainties. Also, the stability is necessary to guarantee the control

system always work with different initial conditions. In this subsection, two Theorems are given to show the stability of the closed-loop system with the finite-time horizon near-optimal controller aforementioned.

Theorem 1. *If $\boldsymbol{S}_0(t)$ is a symmetric positive definite matrix and $\boldsymbol{V}_0(t)$ is a symmetric negative definite matrix, then the cost-to-go function(value function) $J^*(\boldsymbol{x}, t)$ in Eq.(22) is positive-definite and monotonically decreasing to* 0 *with the near-optimal controller of Eq.(23), which is the necessary condition for pointwise stability of the closed system of Eq.(4).*

Proof. Substitute Eq.(25) into Eq.22), $\hat{J}^*(\boldsymbol{x}, t)$ can be written as

$$\hat{J}^*(\boldsymbol{x}, t) = \frac{1}{2}\boldsymbol{x}^{\mathrm{T}}\boldsymbol{S}_0(t)\boldsymbol{x} - \frac{1}{2}\boldsymbol{\nu}^{\mathrm{T}}\boldsymbol{V}_0(t)\boldsymbol{\nu} + \boldsymbol{S}_1^{\mathrm{T}}(t)\boldsymbol{x} + P_1(t) \tag{33}$$

By Remark 3, $\boldsymbol{S}_1 = \boldsymbol{0}$ and $\boldsymbol{P}_1 = 0$, which yields

$$\hat{J}^*(\boldsymbol{x}, t) = \frac{1}{2}\boldsymbol{x}^{\mathrm{T}}\boldsymbol{S}_0(t)\boldsymbol{x} - \frac{1}{2}\boldsymbol{\nu}^{\mathrm{T}}\boldsymbol{V}_0(t)\boldsymbol{\nu} \tag{34}$$

It's obvious that the function $\hat{J}^*(\boldsymbol{x}, t)$ is positive-definite as expressed in Eq.(34). Next, differentiating $\hat{J}^*(\boldsymbol{x}, t)$ and employing the controller and gain differential equations given by Eqs.(23) and (27) yields

$$\begin{aligned}
\dot{\hat{J}}^*(\boldsymbol{x}, t) &= \boldsymbol{x}^{\mathrm{T}}\boldsymbol{S}_0(\boldsymbol{A}\boldsymbol{x} + \boldsymbol{B}\boldsymbol{u}) + \tfrac{1}{2}\boldsymbol{x}^{\mathrm{T}}\dot{\boldsymbol{S}}_0\boldsymbol{x} - \tfrac{1}{2}\boldsymbol{\nu}^{\mathrm{T}}\dot{\boldsymbol{V}}_0\boldsymbol{\nu} \\
&= \boldsymbol{x}^{\mathrm{T}}\boldsymbol{S}_0[\boldsymbol{A}\boldsymbol{x} - \boldsymbol{B}\boldsymbol{R}^{-1}\boldsymbol{B}^{\mathrm{T}}(\boldsymbol{S}_0\boldsymbol{x} + \boldsymbol{P}_0^{\mathrm{T}}\boldsymbol{\nu})] \\
&\quad + \tfrac{1}{2}\boldsymbol{x}^{\mathrm{T}}(-\boldsymbol{Q} + S_0\boldsymbol{B}\boldsymbol{R}^{-1}\boldsymbol{B}^{\mathrm{T}}\boldsymbol{S}_0 - \boldsymbol{S}_0\boldsymbol{A} - \boldsymbol{A}^{\mathrm{T}}\boldsymbol{S}_0)\boldsymbol{x} \\
&\quad - \tfrac{1}{2}\boldsymbol{\nu}^{\mathrm{T}}\boldsymbol{P}_0\boldsymbol{B}\boldsymbol{R}^{-1}\boldsymbol{B}^{\mathrm{T}}\boldsymbol{P}_0^{\mathrm{T}}\boldsymbol{\nu} \\
&= -\tfrac{1}{2}\boldsymbol{x}^{\mathrm{T}}(\boldsymbol{Q} + \boldsymbol{S}_0\boldsymbol{B}\boldsymbol{R}^{-1}\boldsymbol{B}^{\mathrm{T}}\boldsymbol{S}_0)\boldsymbol{x} \\
&\quad - \tfrac{1}{2}\boldsymbol{\nu}^{\mathrm{T}}\boldsymbol{P}_0\boldsymbol{B}\boldsymbol{R}^{-1}\boldsymbol{B}^{\mathrm{T}}\boldsymbol{P}_0^{\mathrm{T}}\boldsymbol{\nu} - \boldsymbol{x}^{\mathrm{T}}\boldsymbol{S}_0\boldsymbol{B}\boldsymbol{R}^{-1}\boldsymbol{B}^{\mathrm{T}}\boldsymbol{P}_0^{\mathrm{T}}\boldsymbol{\nu} \\
&= -\tfrac{1}{2}(\boldsymbol{S}_0\boldsymbol{x} + \boldsymbol{P}_0^{\mathrm{T}}\boldsymbol{\nu})^{\mathrm{T}}\boldsymbol{B}\boldsymbol{R}^{-1}\boldsymbol{B}^{\mathrm{T}}(\boldsymbol{S}_0\boldsymbol{x} + \boldsymbol{P}_0^{\mathrm{T}}\boldsymbol{\nu}) - \tfrac{1}{2}\boldsymbol{x}^{\mathrm{T}}\boldsymbol{Q}\boldsymbol{x}
\end{aligned} \tag{35}$$

where $\boldsymbol{Q} \geqslant 0$ and $\boldsymbol{R} > 0$ is assumed and thus $\dot{\hat{J}}^*(\boldsymbol{x}, t) \leqslant 0$. Furthermore, recalling $\boldsymbol{x} = [\bar{\boldsymbol{q}}^{\mathrm{T}}, \boldsymbol{\omega}^{\mathrm{T}}]^{\mathrm{T}}$, the $\boldsymbol{x}$ cannot be $\boldsymbol{0}$ as $\|\bar{\boldsymbol{q}}\|_2 = 1$. Therefore, $\dot{\hat{J}}^*(\boldsymbol{x}, t) < 0$ for $t \in (t_0, t_{\mathrm{f}})$ implying that $\hat{J}^*(\boldsymbol{x}, t)$ is a monotonically decreasing function and reaches its minimum, namely 0, as it should be. Note that $\boldsymbol{\nu}$ is the terminal Lagrange multiplier and it is a constant whose value is calculated via Eq.(25). □

Theorem 1 implies that the closed-loop system is stable with the preceding optimal controller of Eq.(23). However, even though $\hat{J}^*(\boldsymbol{x}, t_{\mathrm{f}}) = 0$, the terminal value of the state $\boldsymbol{x}$ cannot be determined according to Eq.(34) because $\boldsymbol{S}_0(t_{\mathrm{f}}) = \boldsymbol{0}$ and $\boldsymbol{V}_0(t_{\mathrm{f}}) = \boldsymbol{0}$. The next theorem proves the convergence of the state $\boldsymbol{x}$ to the terminal constraint set of Eq.(15).

Theorem 2. *The state $\boldsymbol{x}$ can reach the terminal constraint set with the proposed controller Eq.(23) if the boundary conditions of gain matrices, namely $\boldsymbol{S}_0(t_{\mathrm{f}}) = \boldsymbol{0}$, $\boldsymbol{V}_0(t_{\mathrm{f}}) = \boldsymbol{0}$, $\boldsymbol{S}_1(t_{\mathrm{f}}) = \boldsymbol{0}$, $\boldsymbol{V}_1(t_{\mathrm{f}}) = -\bar{\boldsymbol{\psi}}_{\mathrm{f}}$, $\boldsymbol{P}_0(t_{\mathrm{f}}) = \bar{\boldsymbol{C}}$, and $P_1(t_{\mathrm{f}}) = 0$ hold.*

Proof. Consider the following Lyapunov-like function candidate:

$$V = -\frac{1}{2}(\boldsymbol{P}_0\boldsymbol{x} + \boldsymbol{V}_1)^{\mathrm{T}}\boldsymbol{V}_0^{-1}(\boldsymbol{P}_0\boldsymbol{x} + \boldsymbol{V}_1) \tag{36}$$

which is a positive definite function because $\boldsymbol{V}_0$ is a symmetric negative definite matrix. The derivative of V is

$$\dot{V} = -(\boldsymbol{P}_0\boldsymbol{x} + \boldsymbol{V}_1)^{\mathrm{T}}\boldsymbol{V}_0^{-1}(\dot{\boldsymbol{P}}_0\boldsymbol{x} + \boldsymbol{P}_0\dot{\boldsymbol{x}} + \dot{\boldsymbol{V}}_1) - \frac{1}{2}(\boldsymbol{P}_0\boldsymbol{x} + \boldsymbol{V}_1)^{\mathrm{T}}\frac{\mathrm{d}\boldsymbol{V}_0^{-1}}{\mathrm{d}t}(\boldsymbol{P}_0\boldsymbol{x} + \boldsymbol{V}_1) \tag{37}$$

Substituting Eqs.(23) and (27) into Eq.(37) yields

$$\dot{V} = (\boldsymbol{P}_0\boldsymbol{x} + \boldsymbol{V}_1)^{\mathrm{T}}\boldsymbol{V}_0^{-1}\boldsymbol{P}_0\boldsymbol{B}\boldsymbol{R}^{-1}\boldsymbol{B}^{\mathrm{T}}\boldsymbol{P}_0^{\mathrm{T}}\boldsymbol{\nu} - \frac{1}{2}(\boldsymbol{P}_0\boldsymbol{x} + \boldsymbol{V}_1)^{\mathrm{T}}\frac{\mathrm{d}\boldsymbol{V}_0^{-1}}{\mathrm{d}t}(\boldsymbol{P}_0\boldsymbol{x} + \boldsymbol{V}_1) \tag{38}$$

Consequently, substitute Eq.(25) into Eq.(38) along with $\frac{\mathrm{dV}_0^{-1}}{\mathrm{dt}} = -\boldsymbol{V}_0^{-1}\dot{\boldsymbol{V}}_0\boldsymbol{V}_0^{-1}$, it follows after some straightforward algebra that

$$\begin{aligned} \dot{V} &= -\tfrac{1}{2}(\boldsymbol{P}_0\boldsymbol{x}+\boldsymbol{V}_1)^{\mathrm{T}}\boldsymbol{V}_0^{-1}\boldsymbol{P}_0\boldsymbol{B}\boldsymbol{R}^{-1}\boldsymbol{B}^{\mathrm{T}}\boldsymbol{P}_0^{\mathrm{T}}\boldsymbol{V}_0^{-1}(\boldsymbol{P}_0\boldsymbol{x}+\boldsymbol{V}_1) \\ &= -\tfrac{1}{2}(\boldsymbol{P}_0\boldsymbol{x}+\boldsymbol{V}_1)^{\mathrm{T}}\boldsymbol{F}(\boldsymbol{P}_0\boldsymbol{x}+\boldsymbol{V}_1) \end{aligned} \tag{39}$$

where the symmetric positive definite matrix $\boldsymbol{V}_0^{-1}\boldsymbol{P}_0\boldsymbol{B}\boldsymbol{R}^{-1}\boldsymbol{B}^{\mathrm{T}}\boldsymbol{P}_0^{\mathrm{T}}\boldsymbol{V}_0^{-1}$ is denoted by $\boldsymbol{F} > 0$ and thus

$$\dot{V} \leqslant -\frac{1}{2}\|\boldsymbol{P}_0\boldsymbol{x}+\boldsymbol{V}_1\|^2\lambda_{\min}(\boldsymbol{F}) \tag{40}$$

which implies that $\|\boldsymbol{P}_0\boldsymbol{x}+\boldsymbol{V}_1\|_2$ converges to 0 as $t \to \infty$. Furthermore, since $\boldsymbol{P}_0(t_{\mathrm{f}}) = \bar{\boldsymbol{C}}$, $\boldsymbol{V}_1(t_{\mathrm{f}}) = -\bar{\boldsymbol{\psi}}_{\mathrm{f}}$, then $\left\|\bar{\boldsymbol{C}}\boldsymbol{x}-\bar{\boldsymbol{\psi}}_{\mathrm{f}}\right\|_2 = 0$ is satisfied as $t_{\mathrm{f}} \to \infty$. The term asymptotic stability for infinite-horizon problems may be used for finite-horizon problems in the sense that as the horizon is extended, the states converge to the terminal constraint set in a fixed time t_{f} [34]. □

Remark 4. Although Theorem 1 and Theorem 2 show the global stability of the system, the nonlinear system Eq.(4) could be only locally stabilizable/controllable because pointwise stability/controllability of $(\boldsymbol{A}(\boldsymbol{x}), \boldsymbol{B}(\boldsymbol{x}))$ does not imply controllability of nonlinear system Eq.(4)[21].

Remark 5. The Theorem 1 and Theorem 2 are exactly correct in the case that the states in the future are known ahead of time. However, as the calculation of the gain matrices in Eq.(27) is an approximate approach, the convergence of the cost-to-go function and the states cannot be rigorously guaranteed.

3.4. Improvement of the SDRE-based near optimal control with a waypoint

The SDRE-based optimal control scheme presented in subsection 3.2 can approximately deal with the fixed time optimal control problem for nonlinear systems. But the SDRE method meets its weakness for large angle maneuvers and

the control performance would degrade seriously because the states in Eq.(27) are frozen at their current values from the current time to final time t_f at each step. To enhance the ability of the SDRE method for handling strong nonlinear optimal control problems, a waypoint method is proposed in this part. A single waypoint at the middle time of t_f is determined by partitioning the original time interval $[t_0, t_\mathrm{f}]$ into two equal parts of $[t_0, t_1^-]$ and $[t_1^+, t_\mathrm{f}]$, $t_1^- = t_1^+ = t_\mathrm{f}/2$. The value of the waypoint $\boldsymbol{x}_1$ is calculated based on the cost-to-go function defined in Eq.(22). For each segment, the end conditions of Eqs.(29) and (31) should be satisfied.

Applying the cost-to-go function defined in Eq.(22), the cost for each segment is

$$\begin{aligned} \hat{J}_1 = \hat{J}^*(t_0, \boldsymbol{x}_0) &= \tfrac{1}{2}{\boldsymbol{x}_0}^\mathrm{T}\boldsymbol{S}_0(t_0)\boldsymbol{x}_0 + \tfrac{1}{2}\boldsymbol{\nu}_0^\mathrm{T}\boldsymbol{V}_0(t_0)\boldsymbol{\nu}_0 \\ &\quad + \boldsymbol{\nu}_0^\mathrm{T}\boldsymbol{P}_0(t_0)\boldsymbol{x}_0 + \boldsymbol{S}_1^\mathrm{T}(t_0)\boldsymbol{x}_0 + \boldsymbol{V}_1^\mathrm{T}(t_0)\boldsymbol{\nu}_0 + P_1(t_0) \end{aligned} \tag{41}$$

$$\begin{aligned} \hat{J}_2 = \hat{J}^*(t_1, \boldsymbol{x}_1) &= \tfrac{1}{2}{\boldsymbol{x}_1}^\mathrm{T}\boldsymbol{S}_0(t_1^+)\boldsymbol{x}_1 + \tfrac{1}{2}\boldsymbol{\nu}_1^\mathrm{T}\boldsymbol{V}_0(t_1^+)\boldsymbol{\nu}_1 \\ &\quad + \boldsymbol{\nu}_1^\mathrm{T}\boldsymbol{P}_0(t_1^+)\boldsymbol{x}_1 + \boldsymbol{S}_1^\mathrm{T}(t_1^+)\boldsymbol{x}_1 + \boldsymbol{V}_1^\mathrm{T}(t_1^+)\boldsymbol{\nu}_1 + P_1(t_1^+) \end{aligned} \tag{42}$$

where $\boldsymbol{x}_1 = \boldsymbol{x}(t_1)$ is an unknown variable to be determined. The total cost is $\hat{J}^* = \hat{J}_1 + \hat{J}_2$.

By using Eq.(25) and $\boldsymbol{S}_1 = \boldsymbol{0}$, $\boldsymbol{P}_1 = 0$ shown in Remark 3 , Eq.(41) can be rewritten as

$$\begin{aligned} \hat{J}_1 &= \tfrac{1}{2}\boldsymbol{x}_0^\mathrm{T}\boldsymbol{S}_0(t_0)\boldsymbol{x}_0 - \tfrac{1}{2}\boldsymbol{\nu}_0^\mathrm{T}\boldsymbol{V}_0(t_0)\boldsymbol{\nu}_0 \\ &= \tfrac{1}{2}x_0^\mathrm{T}\boldsymbol{S}_0(t_0)\boldsymbol{x}_0 - \tfrac{1}{2}[\boldsymbol{P}_0(t_0)\boldsymbol{x}_0 + \boldsymbol{V}_1(t_0)]^\mathrm{T}{\boldsymbol{V}_0}^{-1}(t_0)\,[\boldsymbol{P}_0(t_0)\boldsymbol{x}_0 + \boldsymbol{V}_1(t_0)] \end{aligned} \tag{43}$$

In light of Eqs.(27) and (31), $\boldsymbol{V}_1$ is a constant vector and $\boldsymbol{V}_1(t_0) = \boldsymbol{V}_1(t_\mathrm{f}/2) = -\bar{\boldsymbol{\psi}}_{\mathrm{f}1} = -\boldsymbol{x}_1$ in the first segment of $t \in [0, t_\mathrm{f}/2]$, thus

$$\hat{J}_1 = \frac{1}{2}\boldsymbol{x}_0^\mathrm{T}\boldsymbol{S}_0(t_0)\boldsymbol{x}_0 - \frac{1}{2}[\boldsymbol{P}_0(t_0)\boldsymbol{x}_0 - \boldsymbol{x}_1]^\mathrm{T}{\boldsymbol{V}_0}^{-1}(t_0)\,[\boldsymbol{P}_0(t_0)\boldsymbol{x}_0 - \boldsymbol{x}_1] \tag{44}$$

Likewise, the value function for the second segment is

$$\hat{J}_2 = \frac{1}{2}\boldsymbol{x}_1^{\mathrm{T}}\boldsymbol{S}_0(t_1^+)\boldsymbol{x}_1 - \frac{1}{2}\Big[\boldsymbol{P}_0(t_1^+)\boldsymbol{x}_1 - \bar{\boldsymbol{\psi}}_{\mathrm{f}}\Big]^{\mathrm{T}}\boldsymbol{V}_0{}^{-1}(t_1^+)\Big[\boldsymbol{P}_0(t_1^+)\boldsymbol{x}_0 - \bar{\boldsymbol{\psi}}_{\mathrm{f}}\Big] \tag{45}$$

where $\bar{\boldsymbol{\psi}}_{\mathrm{f}}$ is the state-dependent terminal constraint as shown in Eq.(15). As $\boldsymbol{x}_1$ is the optimal waypoint at the middle of the whole time interval, namely at $t = t_1 = t_{\mathrm{f}}/2$, our goal is to determine the value of $\boldsymbol{x}_1$ to minimize the total cost of $\hat{J}^* = \hat{J}_1 + \hat{J}_2$. Let $\partial\hat{J}^*/\partial\boldsymbol{x}_1 = \boldsymbol{0}$, that is

$$\begin{aligned}\tfrac{\partial\hat{J}^*}{\partial\boldsymbol{x}_1} &= \tfrac{\partial\hat{J}_1}{\partial\boldsymbol{x}_1} + \tfrac{\partial\hat{J}_2}{\partial\boldsymbol{x}_1} \\ &= \Big[-\boldsymbol{V}_0{}^{-1}(t_0) + \boldsymbol{S}_0(t_1^+) - \boldsymbol{P}_0(t_1^+)^{\mathrm{T}}\boldsymbol{V}_0{}^{-1}(t_1^+)\boldsymbol{P}_0(t_1^+)\Big]\boldsymbol{x}_1 \\ &\quad +\boldsymbol{V}_0{}^{-1}(t_0)\boldsymbol{P}_0(t_0)\boldsymbol{x}_0 + \boldsymbol{P}_0(t_1^+)^{\mathrm{T}}\boldsymbol{V}_0{}^{-1}(t_1^+)\bar{\boldsymbol{\psi}}_{\mathrm{f}} = \boldsymbol{0}\end{aligned} \tag{46}$$

from which the value of waypoint $\boldsymbol{x}_1$ can be obtained as

$$\begin{aligned}\boldsymbol{x}_1 &= -\Big[-\boldsymbol{V}_0{}^{-1}(t_0) + \boldsymbol{S}_0(t_1^+) - \boldsymbol{P}_0(t_1^+)^{\mathrm{T}}\boldsymbol{V}_0{}^{-1}(t_1^+)\boldsymbol{P}_0(t_1^+)\Big]^{-1} \\ &\quad \Big[V_0^{-1}(t_0)\boldsymbol{P}_0(t_0)\boldsymbol{x}_0 + \boldsymbol{P}_0(t_1^+)^{\mathrm{T}}\boldsymbol{V}_0{}^{-1}(t_1^+)\bar{\boldsymbol{\psi}}_{\mathrm{f}}\Big]\end{aligned} \tag{47}$$

Then, the calculation for time-varying gain matrices in each segment can be easily conducted by using the backward integration method. Note that for the first segment, the end constraint is a fixed point namely $\boldsymbol{x}(t_1^-) = \boldsymbol{x}_1$, thus the end conditions of gain matrices at $t = t_1 = t_{\mathrm{f}}/2$ are specified as follows:

$$\begin{aligned}&\boldsymbol{S}_0(t_1^-) = \boldsymbol{0}_{7\times7}, \boldsymbol{S}_1(t_1^-) = \boldsymbol{0}_{7\times1}, \boldsymbol{P}_0(t_1^-) = \boldsymbol{I}_{4\times7} \\ &\boldsymbol{V}_0(t_1^-) = \boldsymbol{0}_{4\times4}, \boldsymbol{V}_1(t_1^-) = -\boldsymbol{x}_1, \boldsymbol{P}_1(t_1^-) = 0\end{aligned} \tag{48}$$

But the terminal constraint at $t = t_{\mathrm{f}}$ for the second segment is a nonlinear underdetermined equation, therefore

$$\begin{aligned}&\boldsymbol{S_0}(t_{\mathrm{f}}) = \boldsymbol{0}, \boldsymbol{S}_1(t_{\mathrm{f}}) = \boldsymbol{0}, \boldsymbol{P_0}(t_{\mathrm{f}}) = \bar{\boldsymbol{C}} \\ &\boldsymbol{V_0}(t_{\mathrm{f}}) = \boldsymbol{0}, \boldsymbol{V}_1(t_{\mathrm{f}}) = -\bar{\boldsymbol{\psi}}_{\mathrm{f}}, \boldsymbol{P}_1(t_{\mathrm{f}}) = 0\end{aligned} \tag{49}$$

where $\bar{\boldsymbol{C}}$ and $\bar{\boldsymbol{\psi}}_{\mathrm{f}}$ are shown in Eq.(15). The procedure of the SDRE approach with a waypoint is illustrated as follows:

Step 1: Calculate waypoint $\boldsymbol{x}_1$.

Step 2: If $t < t_{\mathrm{f}}/2$, calculate end conditions by Eq.(48), else by Eq.(49).

Step 3: Gain matrices calculation by Eq.(27).

Step 4: Update control law $\boldsymbol{u}$ via Eq.(23), go back to step 2.

It should be noted that the waypoint-based SDRE approach not only enhances the control performance and optimality for repointing maneuver but reduces the computation burden compared with the traditional SDRE method. The computational complexity of the time-varying gain matrices in Eq.(27) depends on the maneuver time t_{f} and the time step size h_s (control period) since the total control steps $N_s = t_{\mathrm{f}}/h_s$. For each step, in order to obtain the value of the gain matrices, the backward integration from the final time to the current time needs to be conducted. Denote the integration step is h_i and the current time is t, the number of total integration steps in each control period is $N_i = (t_{\mathrm{f}} - t)/h_i$. The total integration steps from $t_0 = 0$ to t_{f} for the traditional SDRE approach can be obtained as

$$N_{\mathrm{total}} = \frac{N_s t_{\mathrm{f}}}{h_i} - \frac{h_s}{h_i}\frac{(1+N_s)N_s}{2} = \frac{{t_{\mathrm{f}}}^2}{h_s h_i} - \frac{t_{\mathrm{f}}}{h_i}\frac{(1+t_{\mathrm{f}}/h_s)}{2} = \frac{{t_{\mathrm{f}}}^2 - t_{\mathrm{f}} h_s}{2h_s h_i} \tag{50}$$

while the total integration steps for the waypoint-based SDRE is

$$N_{\mathrm{total}}^{'} = \frac{{t_{\mathrm{f}}}^2}{2h_s h_i} - \frac{t_{\mathrm{f}}}{h_i}\frac{(1+t_{\mathrm{f}}/2h_s)}{2} = \frac{2{t_{\mathrm{f}}}^2 - t_{\mathrm{f}}(2h_s + t_{\mathrm{f}})}{4h_s h_i} = \frac{{t_{\mathrm{f}}}^2 - 2t_{\mathrm{f}} h_s}{4h_s h_i} \tag{51}$$

Since $h_s \ll t_{\mathrm{f}}$, the total computation time of the traditional SDRE method and the waypoint-based SDRE approach is basically proportional to ${t_{\mathrm{f}}}^2/h_s h_i$, namely $T_{\mathrm{total}} \propto \frac{{t_{\mathrm{f}}}^2}{h_s h_i}$. Comparing Eqs. (50) with (51) yields

$$N_{\mathrm{total}} - N_{\mathrm{total}}^{'} = \frac{{t_{\mathrm{f}}}^2}{4h_s h_i} > 0 \tag{52}$$

which implies that the waypoint-based SDRE approach is more computationally efficient than traditional SDRE approach. The numerical simulations for different maneuver time t_{f} and the step size h_s are performed to test the computation time. All computations are performed on an Intel(R) Core(TM) i7-4770 CPU desktop machine with a 3.4GHz processor and 8 GB of RAM. The simulation results are shown in Table 1. Note that the maneuver time t_{f} and the step size h_s should be properly selected to ensure that the total computation time T is shorter than t_{f}. Otherwise, the repointing maneuver would not be realized in a fixed time t_{f}.

Table 1: Computation time for different maneuver time and step size

Maneuver time t_{f}(s)	Simulation step size h_s(s)	Integration step size h_i(s)	Computation time without the waypoint T_{SDRE}(s)	Computation time with the waypoint T_{WSDRE}(s)
10	0.1	0.1	0.69	0.44
10	0.05	0.05	2.55	1.02
10	0.01	0.01	60.38	30.45
15	0.1	0.1	1.44	0.59
15	0.05	0.05	5.66	2.19
15	0.01	0.01	136.84	50.90
20	0.1	0.1	2.49	1.03
20	0.05	0.05	9.89	4.13
20	0.01	0.01	240.48	92.60

4. Numerical Simulations

Various numerical simulation results for fixed-time repointing maneuver of the spacecraft with zero and nonzero terminal angular velocity are presented in this section to illustrate the validity of the SDRE-based method developed in the preceding sections.

The inertia matrix was selected as $\boldsymbol{J}_{\mathrm{s}} = \begin{bmatrix} 86.24 & 0 & 0 \\ 0 & 85.07 & 0 \\ 0 & 0 & 113.59 \end{bmatrix}$.

The weight matrices for the cost function in Eq.(13) are $\boldsymbol{Q} = \mathrm{diag}[1, 1, 1, 1, 4, 4, 4]$, $\boldsymbol{R} = \mathbf{I}_{3\times3}$, the final time $t_{\mathrm{f}} = 10$s. Initial conditions are selected as

$$\boldsymbol{x}_{t_0} = [q_{10}, q_{20}, q_{30}, q_{40}, \omega_{10}, \omega_{20}, \omega_{30}] = [0, 0, 0, 1, 0, 0, 0]$$

The target orientation $\boldsymbol{t}$ expressed in the inertial frame is $\boldsymbol{t}^{\mathrm{i}} = [2\ 1\ 1]^{\mathrm{T}}/\sqrt{6}$, and the X_{b} axis needs to be aligned with $\boldsymbol{t}$ in the end. The weight matrix $\boldsymbol{Q} = \mathrm{diag}[Q_{q_1}, Q_{q_2}, Q_{q_3}, Q_{q_4}, Q_{\omega_1}, Q_{\omega_2}, Q_{\omega_3}]$ decides the penalty on $\boldsymbol{x}$ while $\boldsymbol{R} = \mathrm{diag}[R_1, R_2, R_3]$ puts the penalty on $\boldsymbol{u}$. The value of $\boldsymbol{Q}$ and $\boldsymbol{R}$ influences the trajectories of the control torque and states. Considering $\boldsymbol{x} = [q_1, q_2, q_3, q_4, \omega_1, \omega_2, \omega_3]^{\mathrm{T}}$, since the integral of the quaternion has no practical meaning, $Q_{q_1} = Q_{q_2} = Q_{q_3} = Q_{q_4} = \delta$(constant) should be satisfied to make $Q_{q_1}q_1^2 + Q_{q_2}q_2^2 + Q_{q_3}q_3^2 + Q_{q_4}q_4^2 = \delta$ so that it doesn't influence the control results. Q_{ω_1} , Q_{ω_2} and Q_{ω_3} produces a damping effect for the closed-loop system like that in PID control and the larger Q_{ω_i} brings about the smaller torque u_i while the larger R_i also generates the smaller control torque u_i. Note that to realize repointing maneuver at a fixed time, the torque decrease along one body-fixed axis must brings about a torque increase around other axes.

In practice, the engineer should design the weight matrices of $\boldsymbol{Q}$ and $\boldsymbol{R}$ properly based on the real mission and the actuators ability. For instance, if the maximum

output torque along Z_b axis is smaller than that along the other two axis, then R_3 and Q_{ω_3} should be set to a value larger than R_1 , R_2 and Q_{ω_1} , Q_{ω_2} respectively.

*4.1. **Repointing maneuver with zero terminal angular velocity***

A. SDRE-based method without a waypoint

To start with, the problem of stationary targets detection is examined by using the SDRE method presented in subsection 3.2 without the waypoint. The terminal constraints can be derived from Eq.(12).

The simulation results are depicted in Fig.1-Fig.5. In Fig.1 and Fig.2, the attitude trajectories of the spacecraft are given where the solid lines denote the SDRE-based results and the dashed lines denote the results of the GPOPS[35] which can be deemed as the real optimal solutions. The control torque histories are illustrated in Fig. 3 where u_1, u_2 and u_3 represents the control torque along three body axis respectively. The difference between u_1 and u_1^* is clear. As can be seen from Fig. 4, around 10s into the simulation, the pointing error angle p_e starts off near 35° and successfully converges to 10^{-5°. In Fig. 5, the trajectories of the cost-to-go is given. The solid line represents the quadratic cost-to-go function J_c^* designed in Eq.(22) that is an approximation to the real cost-to-go J_r^* based on SDRE method which is plotted by the dotted line. The difference between J_c^* and J_r^* results from the approximations considered in the method itself for successive linearization of the terminal curve constraint and attitude kinematics with respect to the current state. Note that nether J_c^* nor J_r^* can represent the real optimal solution J^* of GPOPS (dash line), as they are both based on the SDRE method proposed in this paper. It shows that the overall cost of repointing maneuver defined in Eq.(13) by using SDRE-based method is $J_r^*(t_0) = 28.3$, while the real optimal solution is $J^*(t_0) = 27.68$.

Furthermore, the accuracy of the methodology is examined with different initial conditions. The numerical results are recorded in Table 2 where the slew angle Φ denotes the angle between the initial body X_b axis and target orientation. For small slew angles, the SDRE-based optimal control approach performs well and the performance index is very close to that of real optimal solution. However, the SDRE-based method may become unattractive if slew angles are larger than 90° because the spacecraft requires to maneuver faster to realize repointing maneuver in fixed time, which strengthens the coupling between three body axis, thus the pointwise linearization cannot ensure the optimality. The loss of optimality is calculated by $(J^*_{\mathrm{SDRE}} - J^*)/J^* \times 100\%$. Even though the SDRE-based method is not optimal for large angle maneuvers, the control accuracy is high and not getting worse seriously for large slew angles. The pointing error is within 10^{-3}°. To illustrate the results more intuitively, the attitude trajectories for different initial conditions are given in Fig.6 where the blue circle is the terminal attitude constraint defined in Eq.(12) for the given target orientation $\boldsymbol{t}^\mathrm{i} = [2\ 1\ 1]^\mathrm{T}/\sqrt{6}$. It shows that the quaternions can reach the ring-shaped terminal constraint set in the end wherever they start.

B. Improved SDRE-based method with a waypoint

The traditional SDRE-based approach presented in subsection 3.2 could realize suboptimal control for repointing maneuver with a good performance. However, the control performance would be discounted seriously along with the increase of maneuver angles. The comparison of the traditional SDRE method and the waypoint-based SDRE approach proposed in subsection 3.4 is conducted in this part. Suppose that the target direction is $\boldsymbol{t}^\mathrm{i} = [1\ 3\ 1]^\mathrm{T}/\sqrt{11}$, thus the initial angle between the optical axis X_b and the $\boldsymbol{t}$ is 72.5°.

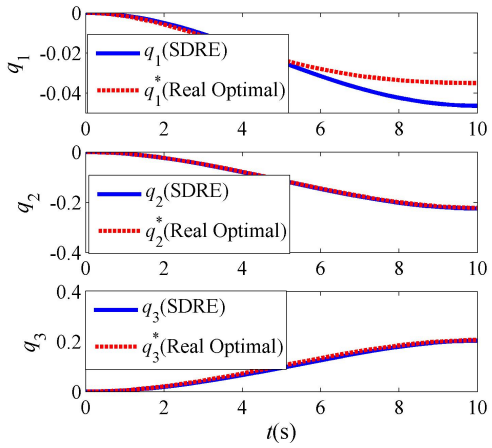

Figure 1: Quaternion trajectories by using SDRE method

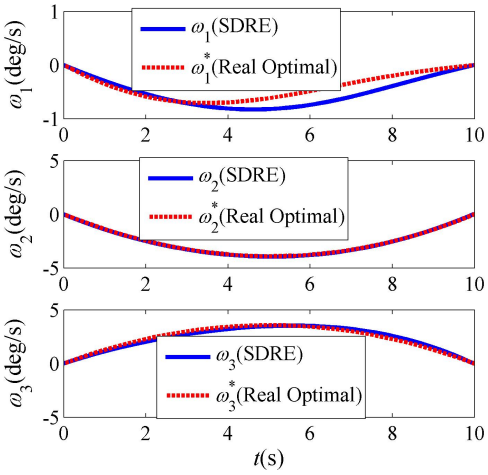

Figure 2: Angular velocities by using SDRE method

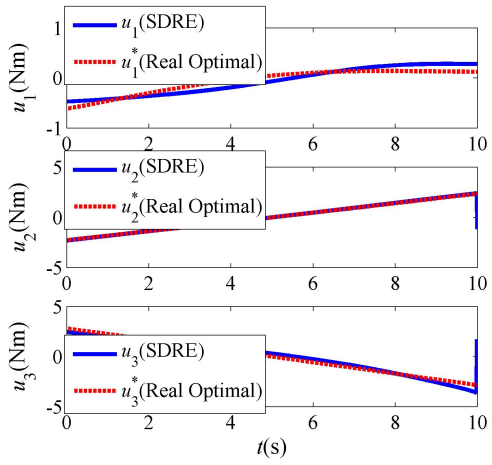

Figure 3: Control trajectories for SDRE method

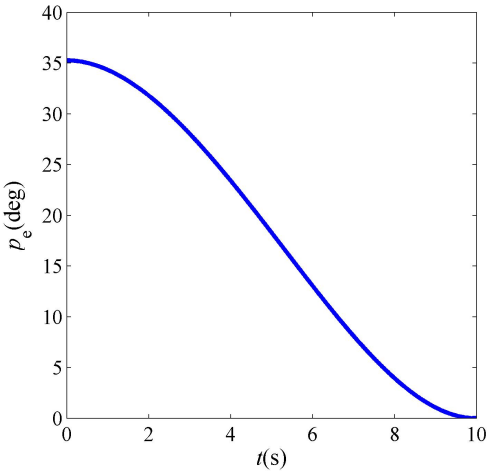

Figure 4: Pointing error trajectory by using SDRE method

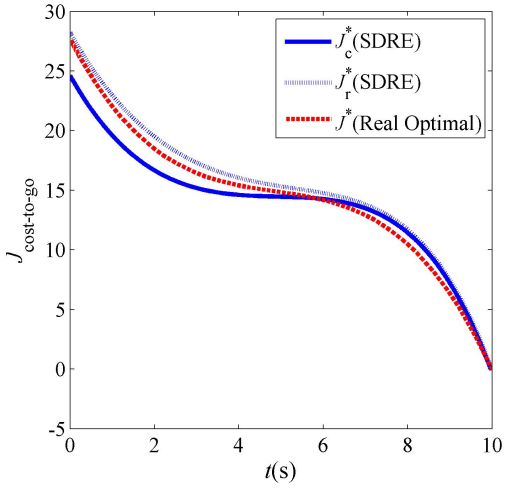

Figure 5: Different cost-to-go functions

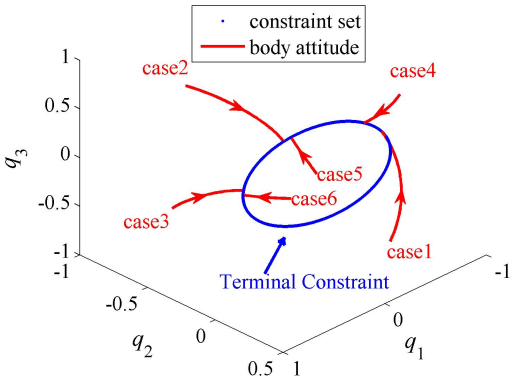

Figure 6: Quaternion trajectories for different initial conditions by using SDRE method

Table 2: Cost index and pointing error with respect to different initial conditions

Initial quaternion $\boldsymbol{q}_0$	slew angle $\Phi(\circ)$	Pointing error $(\circ)$	Near optimal index J^*_{SDRE}	Real optimal index J^*	Loss of optimality(%)
[0.4 0.2 0.2 0.9]	13.6	2.2×10^{-5}	7.79	7.77	0.26
[0.36 $-$ 0.18 0.45 0.8]	22.1	3.74×10^{-5}	16.62	16.53	0.55
[0 0 0 1]	35.3	5.8×10^{-5}	28.3	27.7	2.17
[0.31 $-$ 0.31 0.55 0.71]	44	8.4×10^{-5}	50.64	49.38	2.55
[0.63 0.32 0.63 0.32]	55.1	1.2×10^{-4}	47.83	45.7	4.66
[$-$0.82 0 0.41 0.41]	65.9	1.62×10^{-4}	110.7	95.8	15.55
[0.23 $-$ 0.72 0.34 0.57]	78	2.27×10^{-4}	119.7	93.2	28.43
[0.85 $-$ 0.43 $-$ 0.21 0.21]	87.9	3.07×10^{-4}	187.0	121.6	55.82
[0.43 $-$ 0.43 0.76 0.22]	96	3.74×10^{-4}	337.5	216.6	55.82
[$-$0.5 0.17 $-$ 0.83 0.17]	103.1	4.9×10^{-4}	329.3	158.9	107.23

As can be seen from Fig.8, the angular velocity ω_3 along the Z_b axis is larger than ω_2 along Y_b axis for our proposed improved SDRE method with a waypoint(solid line), which is more similar to the real optimal results(dashed line) than the classical SDRE method(dotted line). The control torque trajectories for different control methods are illustrated in Fig.9. There exists one control switch at t=5s for the improved SDRE method as the two segments partitioned by the waypoint are relatively independent when calculating the control torque thereby resulting in $\boldsymbol{u}(t_1^-) \neq \boldsymbol{u}(t_1^+)$. The superiority of the waypoint over the traditional SDRE approach is shown in Fig.11 which depicts the trajectories of the cost-to-go function. As analyzed previously, the optimality performance of the SDRE method degrades for large angle maneuver. The total performance index of the traditional SDRE method is 147, much higher than the optimal one which is 120.8. The waypoint method can improve the control performance to a great extent of which the total cost is 127.3.

To further illustrate the feasibility of the waypoint-based SDRE approach for large angle maneuvers, the performance index for different target orientations is listed in Table 3. Note that for large angle maneuvers, the maneuver time should be set larger considering the actuators' ability in practice. Thus the maneuver time is set as t=20s when maneuver angle $\Phi > 90^\circ$. The traditional SDRE approach can not apply the near optimal solutions for large angle maneuvers as shown in the 5th column of Table 3 because the frozen coefficients strategy in backward integration process leads to large deviations in the beginning, thus the control torque would be adjusted rapidly to realize repointing maneuver in the last few seconds which gives rise to large control torques and angular velocities as shown in Fig.12 and Fig.13. Although the waypoint can improve the optimality of the SDRE method,

it performs not well enough when $\Phi > 90°$. The reason for this is that when the target direction is far away from the initial X_b axis, the SDRE method can not be capable to select the most suitable path for repointing maneuver, even though with a waypoint.

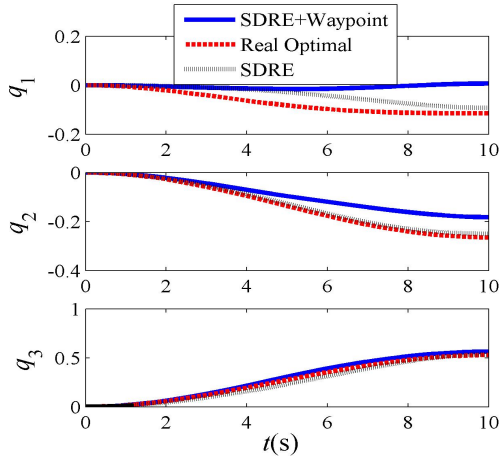

Figure 7: Quaternion trajectories by using different controllers

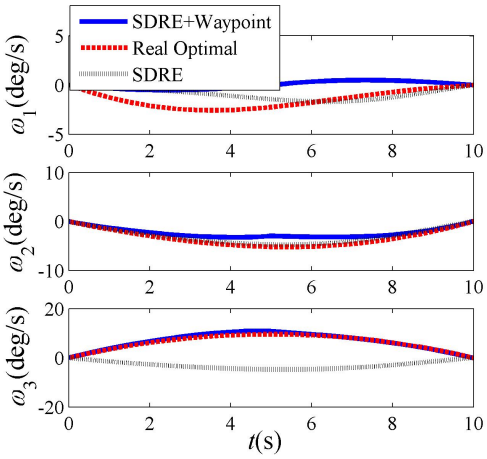

Figure 8: Angular velocities by using different controllers

*4.2. **Repointing maneuver with nonzero terminal angular velocity***

The terminal angular velocity $\boldsymbol{\omega}_f^i$ of the spacecraft expressed in the inertial frame can be determined according to the targets speed $\boldsymbol{v}_f$ at $t = t_f$ and generally $\boldsymbol{\omega}_f^i$ should be perpendicular to the target orientation $\boldsymbol{t}^i = [2\ 1\ 1]^T/\sqrt{6}$ as shown in Fig.14. The value of $\boldsymbol{\omega}_f^i$ is set as $\boldsymbol{\omega}_f^i = [0.1\ -0.1\ -0.1]^T$rad/s.

Fig.15 illustrates that the attitude trajectory of the spacecraft using the waypoint-based SDRE approach is closer to the optimal results. The optical axis X_b points to the target at $t = 10$s with a given angular velocity of $\boldsymbol{\omega}_f^i = [5.7\ -5.7\ -5.7]^T°/$s which is expressed in the inertial frame as expected shown in Fig.16 and Fig. 18.

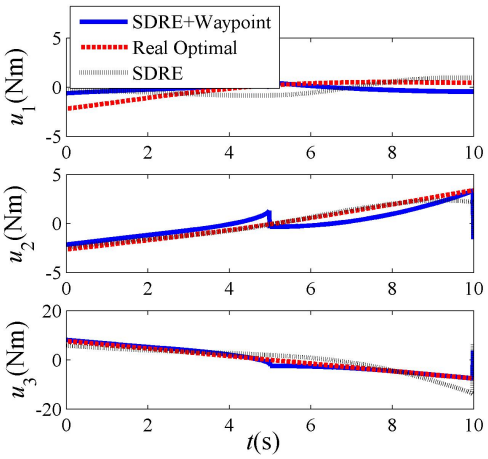

Figure 9: Control trajectories for different controllers

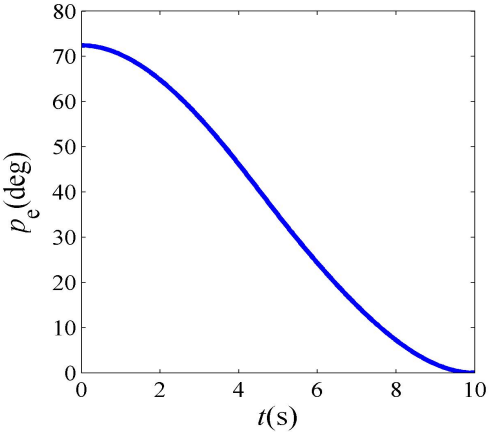

Figure 10: Pointing error trajectory by using waypoint-based SDRE method

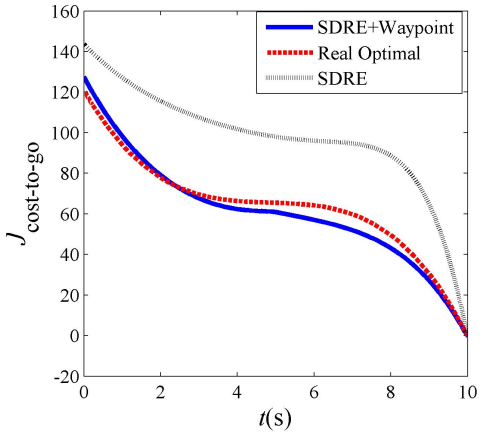

Figure 11: History of cost-to-go functions for different controllers

Table 3: Comparison of cost index for different target orientations

Target orientation $\boldsymbol{t}$	slew angle $\Phi(\circ)$	Maneuver time(s)	Performance index with waypoint J_{WSDRE}	Performance index without waypoint J_{SDRE}	Real optimal index J^*
$[0.19, 0.96, 0.19]$	78.9	10	154.4	201	147.8
$[0.15, 0.88, 0.44]$	81.5	10	168.8	215.8	140.6
$[0.12, 0.96, 0.24]$	83.1	10	170.8	233.8	160.2
$[-0.26, 0.53, 0.8]$	105.5	20	52.23	64.4	31.2
$[-0.49, 0.49, 0.73]$	119.0	20	72.5	118.1	36.4
$[-0.57, 0.57, 0.57]$	125.3	20	73.5	188.6	40.9
$[-0.78, 0.2, 0.59]$	141.6	20	153.9	401.1	44.6
$[-0.82, 0.41, 0.41]$	144.7	20	106.7	762.5	78.6
$[-0.94, 0.24, 0.24]$	160.5	20	140.5	**4889**	79.7
$[-0.97, 0.16, 0.16]$	166.7	20	156.4	**16187**	80

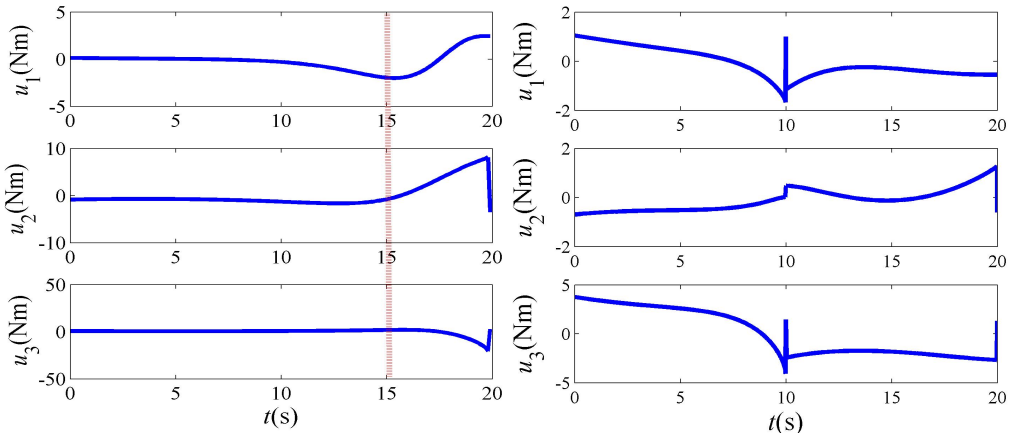

(a)without the waypoint (b)with a waypoint

Figure 12: Comparison of control trajectories for $\boldsymbol{t}$=[-0.57,0.57,0.57]$^{\text{T}}$

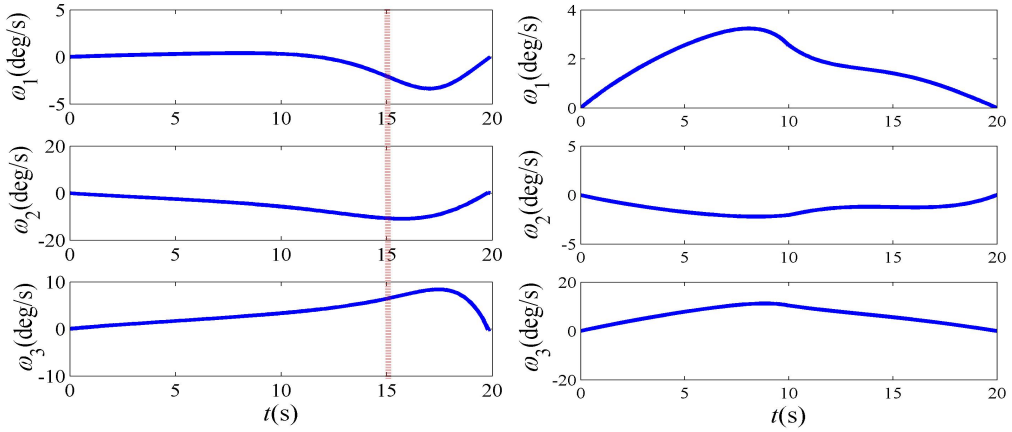

(a)without the waypoint (b)with a waypoint

Figure 13: Comparison of angular velocities for $\boldsymbol{t}$=[-0.57,0.57,0.57]$^{\mathrm{T}}$

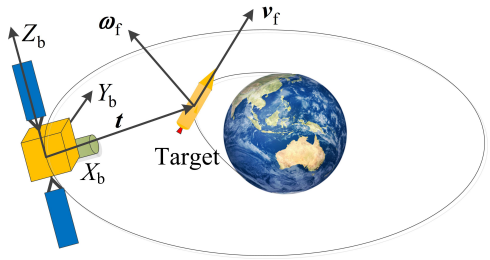

Figure 14: Diagrammatic sketch of moving target detection

The near-optimal solutions based on the waypoint method is closer to the real-optimal solutions in terms of control and attitude trajectories as well as the cost-to-go functions. We can see from Fig.20 that the overall cost defined in Eq.(13) by using traditional SDRE-based method is $J_{\mathrm{SDRE}}(t_0) = 100$, while the waypoint-based SDRE approach is $J_{\mathrm{WSDRE}}(t_0) = 94$ that is closer to the real optimal index $J^* = 89$.

Likewise, when the maneuver angle is large, the traditional SDRE method performs so bad that the control torque and angular velocities in the last few seconds are extremely large as shown in Fig. 21 and Fig. 22.

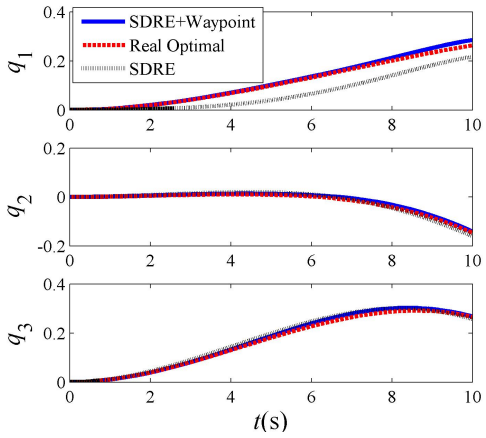

Figure 15: Quaternion trajectories for moving target observation

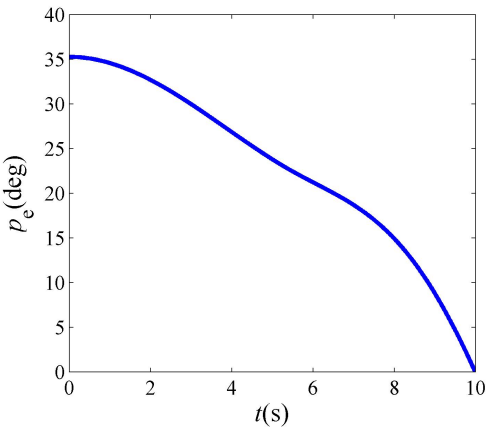

Figure 16: Pointing error trajectory for moving target observation

5. Conclusions

This paper addresses the problem of fixed-time optimal control for a repointing maneuver of a spacecraft operating in staring mode. Both of the attitude and angular velocity terminal constraints are formulated as a group of under-determined

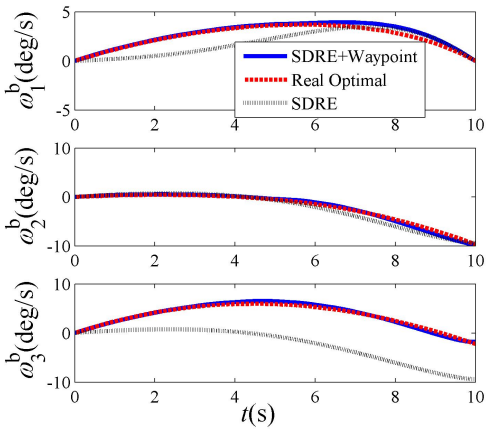

Figure 17: Angular velocities in the body frame for moving target observation

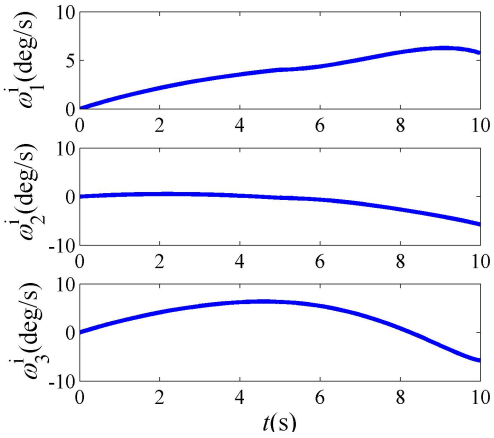

Figure 18: Angular velocities in the inertial frame for moving target observation

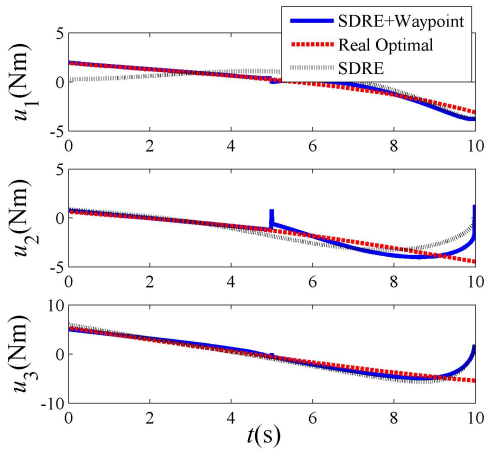

Figure 19: Control trajectories for moving target observation

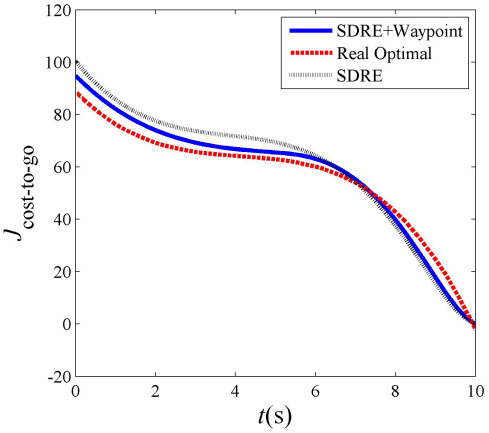

Figure 20: History of cost-to-go functions for moving target observation

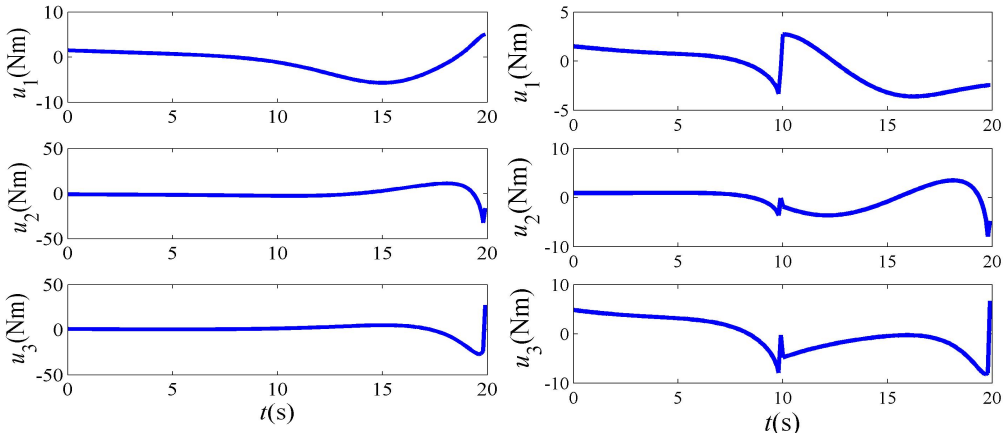

(a)without the waypoint (b)with a waypoint

Figure 21: Comparison of control trajectories for moving target observation with $\boldsymbol{t}=[-0.57,0.57,0.57]^{\mathrm{T}}$

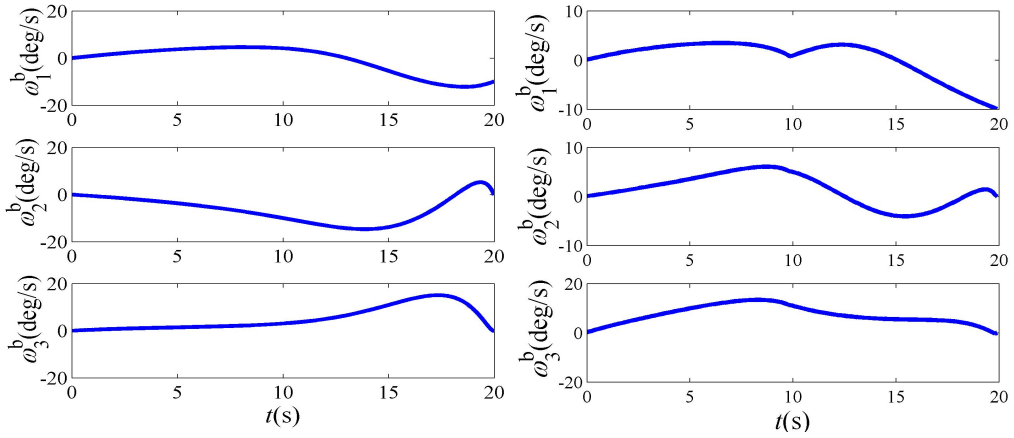

(a)without the waypoint (b)with a waypoint

Figure 22: Comparison of angular velocities for moving target observation with $\boldsymbol{t}=[-0.57,0.57,0.57]^{\mathrm{T}}$

nonlinear equations. This problem can be framed as a nonlinear optimal control problem with nonlinear terminal constraints. This problem is solved by using a newly established SDRE-based dynamic programming approach. The method overcomes the sensitivity issues to uncertainties inherent in open-loop planning as well as being simple to implement. Moreover, an improved SDRE approach which includes waypoint setting is presented which performs better than the traditional SDRE method in terms of control performance and computational efficiency.

The simulation results and comparisons demonstrate that the waypoint-based SDRE approach is superior for large angle maneuvers of the spacecraft in terms of control performance and computation efficiency. In future work, a prediction-based error correction approach should be studied for gain matrix calculation which would reduce the control errors and enhance the optimality. Furthermore, only one waypoint is considered in this paper. The multi-waypoints method should be pursued in the future.

Acknowledgment

This work is supported by the National Natural Science Foundation of China (Grants No. 61876050 and 61673135).

References

[1] S. Roemer, U. Renner, Flight experiences with dlr-tubsat, Acta Astronautica 52 (9-12) (2003) 733–738.

[2] M. Buhl, T. Segert, B. Danziger, Tubsatła reliable and cost effective micro satellite platform, in: 61st International Astronautical Congress, 2010.

[3] K. Cui, J. Xiang, Variable coefficients pd adaptive attitude control of video satellite for ground multi-object staring imaging, in: ELECTRICAL ENGINEERING AND AUTOMATION: Proceedings of the International Conference on Electrical Engineering and Automation (EEA2016), World Scientific, 2017, pp. 738–750.

[4] S. Wu, X. Sun, Z. Sun, X. Wu, Sliding-mode control for staring-mode spacecraft using a disturbance observer, Proceedings of the Institution of Mechanical Engineers, Part G: Journal of Aerospace Engineering 224 (2) (2010) 215–224.

[5] K. Cui, J. Xiang, Y. Zhang, Mission planning optimization of video satellite for ground multi-object staring imaging, Advances in Space Research 61 (6) (2018) 1476–1489.

[6] Y. Lian, Y. Gao, G. Zeng, Staring imaging attitude control of small satellites, Journal of Guidance, Control, and Dynamics 40 (5) (2017) 1278–1285.

[7] C. M. Pong, D. W. Miller, Reduced-attitude boresight guidance and control on spacecraft for pointing, tracking, and searching, Journal of Guidance, Control, and Dynamics 38 (6) (2015) 1027–1035.

[8] Y. Yang, Quaternion-based lqr spacecraft control design is a robust pole assignment design, Journal of Aerospace Engineering 27 (1) (2012) 168–176.

[9] G. Elnagar, M. A. Kazemi, M. Razzaghi, The pseudospectral legendre method for discretizing optimal control problems, IEEE transactions on Automatic Control 40 (10) (1995) 1793–1796.

[10] W. Cai, L. Yang, Y. Zhu, Optimal reorientation of asymmetric underactuated spacecraft using differential flatness and receding horizon control, Advances in Space Research 55 (1) (2015) 343–353.

[11] N. Adurthi, P. Singla, M. Majji, Sparse approximation–based collocation scheme for nonlinear optimal feedback control design, Journal of Guidance, Control, and Dynamics 40 (2) (2016) 248–264.

[12] R. Bellman, 1957, dynamic programming. princeton university press, princeton, n. j.

[13] R. W. Beard, G. N. Saridis, J. T. Wen, Galerkin approximations of the generalized hamilton-jacobi-bellman equation, Automatica 33 (12) (1997) 2159–2177.

[14] H. S. Nik, S. Effati, M. Shirazian, An approximate-analytical solution for the hamilton–jacobi–bellman equation via homotopy perturbation method, Applied Mathematical Modelling 36 (11) (2012) 5614–5623.

[15] B. Kafash, A. Delavarkhalafi, S. Karbassi, Application of variational iteration method for hamilton–jacobi–bellman equations, Applied Mathematical Modelling 37 (6) (2013) 3917–3928.

[16] J. Pearson, Approximation methods in optimal control i. sub-optimal control, International Journal of Electronics 13 (5) (1962) 453–469.

[17] H. Beikzadeh, H. D. Taghirad, Robust sdre filter design for nonlinear uncertain systems with an h performance criterion, ISA transactions 51 (1) (2012) 146–152.

[18] T. Cimen, Survey of state-dependent riccati equation in nonlinear optimal feedback control synthesis, Journal of Guidance, Control, and Dynamics 35 (4) (2012) 1025–1047.

[19] Y. Liang, L. Lin, Analysis of sdc matrices for successfully implementing the sdre scheme, Automatica 49 (10) (2013) 3120–3124.

[20] L. Lin, J. Vandewalle, Y. Liang, Analytical representation of the state-dependent coefficients in the sdre/sddre scheme for multivariable systems, Automatica 59 (2015) 106–111.

[21] K. D. Hammett, C. D. Hall, D. B. Ridgely, Controllability issues in nonlinear state-dependent riccati equation control, Journal of guidance, control, and dynamics 21 (5) (1998) 767–773.

[22] L. Guarnaccia, R. Bevilacqua, S. P. Pastorelli, Suboptimal lqr-based spacecraft full motion control: Theory and experimentation, Acta Astronautica 122 (2016) 114–136.

[23] Z. Xu, X. Chen, Y. Huang, Y. Bai, W. Yao, Nonlinear suboptimal tracking control of spacecraft approaching a tumbling target, Chinese Physics B 27 (9) (2018) 090501.

[24] N. Wang, H. R. Karimi, H. Li, S. Su, Accurate trajectory tracking of disturbed surface vehicles: A finite-time control approach, IEEE/ASME Transactions on Mechatronics.

[25] M. H. Korayem, S. R. Nekoo, Nonlinear optimal control via finite time horizon state-dependent riccati equation, in: 2014 Second RSI/ISM International

Conference on Robotics and Mechatronics (ICRoM), IEEE, 2014, pp. 878–883.

[26] M. Korayem, S. Nekoo, Finite-time state-dependent riccati equation for time-varying nonaffine systems: Rigid and flexible joint manipulator control, ISA transactions 54 (2015) 125–144.

[27] A. Heydari, S. Balakrishnan, Path planning using a novel finite horizon suboptimal controller, Journal of guidance, control, and dynamics 36 (4) (2013) 1210–1214.

[28] A. Heydari, S. Balakrishnan, Closed-form solution to finite-horizon suboptimal control of nonlinear systems, International Journal of Robust and Nonlinear Control 25 (15) (2015) 2687–2704.

[29] A. Bryson, Y. C. Ho, Applied optimal control hemisphere washington (1975).

[30] S. R. Vadali, R. Sharma, Optimal finite-time feedback controllers for nonlinear systems with terminal constraints, Journal of Guidance, Control, and Dynamics 29 (4) (2006) 921–928.

[31] R. Sharma, G. W. York, Near optimal finite-time terminal controllers for space trajectories via sdre-based approach using dynamic programming, Aerospace Science and Technology 75 (2018) 128–138.

[32] J. Sun, C. Liu, Backstepping-based adaptive predictive optimal control of nonlinear systems with application to missile–target engagement, ISA transactions 83 (2018) 42–52.

[33] J. Zhang, H. Zhang, Z. Liu, Y. Wang, Model-free optimal controller design for continuous-time nonlinear systems by adaptive dynamic programming based on a precompensator, ISA transactions 57 (2015) 63–70.

[34] D. Adhyaru, I. Kar, M. Gopal, Fixed final time optimal control approach for bounded robust controller design using hamilton–jacobi–bellman solution, IET control theory & applications 3 (9) (2009) 1183–1195.

[35] M. A. Patterson, A. V. Rao, Gpops-ii: A matlab software for solving multiple-phase optimal control problems using hp-adaptive gaussian quadrature collocation methods and sparse nonlinear programming, ACM Transactions on Mathematical Software (TOMS) 41 (1) (2014) 1.